Surface Segregation in Binary Polymer Blends due to Stiffness Disparity

by

Melika Keymanesh

A thesis

presented to the University of Waterloo

in fulfillment of the

thesis requirement for the degree of

Master of Science

in

Chemical Engineering

Waterloo, Ontario, Canada, 2021

Author's Declaration

I hereby declare that I am the sole author of this thesis. This is a true copy of the thesis, including any required final revisions, as accepted by my examiners.

I understand that my thesis may be made electronically available to the public.

Abstract

The main objective of this work is to study the surface segregation of a binary polymer blend, where the two components have the same molecular volume but are different in other properties such as end-to-end distance, stiffness, and length. Two models are used to represent the polymer chain, which are known as the Gaussian chain model and the worm-like chain model. Working with the Gaussian chain model, the only parameter is the end-to-end distance and it is shown that the surface is rich in the polymer with a shorter end-to-end distance.

Working with the worm-like chain model, we have the ability to change persistence and contour length individually. Hence, we can determine if the polymer has a large end-to-end distance, which of these parameters is responsible for that. This is a better model to predict polymer behavior especially as the polymer gets stiffer. However, it involves more complicated calculations.

The results for this model show that if two polymers have the same persistence length, the shorter polymer segregates to the surface. On the other hand, if the two components have the same chain length, the polymer with a shorter persistence length segregates to the surface.

The other objective of this work is to compare the two mentioned models. In order to do so, I consider a binary polymer blend, where two components have the same end-to-end distance but their persistence length and contour length are different. According to the Gaussian chain model, there would be no segregation in the polymer blend, but the worm-like chain model showed that the shorter and stiffer component segregates to the surface. This difference between the results shows that the Gaussian chain model has some limitations which are well illustrated in the thesis.

Acknowledgements

I would like to express my deepest appreciation to my supervisor, professor Mark Matsen. This work was not possible without his unwavering support. Besides, I would like to express my sincere thanks to Dr. Russell Spenser who helped me a lot with coding and explaining general concepts in polymer physics. Finally, I gratefully acknowledge the assistance of Dr. Pendar Mahmoudi for her background work in this field, which gave me an invaluable insight about polymer surface segregation.

Dedication

I dedicate this thesis to my parents, who taught me how to love and how to be loved, and supported me by all their powers even though they were far from me.

In addition, I would like to dedicate this work to all my professors, especially professor Mark Matsen and professor Bijan Rahimi, for their great effort in teaching me critical thinking and problem-solving.

Table of Contents

List of Figures

List of Abbreviations

SCFT	Self-Consistent Field Theory
MD	Molecular Dynamics
MC	Monte Carlo
PDI	polydispersity index
FWHM	Full Width at Half Maximum

List of Symbols

z	distance from the surface
ξ	width of the surface
R_0	end-to-end distance
s	backbone parameter
w	external field
D	the box size
q	partition function
Q_i	single chain partition function for component i
ϕ_{ref}	reference concentration
ϕ_i	concentration of component i
n	total number of polymers in the blend
$\delta\phi$	excess concentration
$\bar{\phi}$	bulk concentration

Θ_{ex}	integrated excess
ρ_0	bulk segment density
ℓ_c	contour length
ℓ_p	persistence length
$\mathbf{u}$	tangent vector
$\mathbf{R}$	position vector
R_{avg}	average end-to-end distance of two components
ΔR	difference of two end-to-end distances
N_i	number of molecules with molecular weight equal to M_i
M_i	molecular weight of component i
$\bar{M}_n$	number average molecular weight
$\bar{M}_w$	weight average molecular weight
$\bar{M}_v$	viscosity average molecular weight
$\bar{M}_z$	z-average molecular weight
c_i	weight of component i
ΔG_m	mixing free energy
ΔH_m	mixing enthalpy
ΔS_m	mixing entropy

T	temperature
$\Phi_{\max}$	peak height of the excess concentration profile
z_{bulk}	point that concentration reaches to the bulk concentration
a	segment length
n	degree of polymerization

Chapter 1

Introduction

Polymers are large molecules, which have various properties that make them useful. They are lightweight while still significantly strong. They are also processable and posses characteristics such as softness, transparency, electrical and thermal insulation and resistance to chemicals.

Polymeric materials are widely used in different technological and scientific fields [3, 4, 5]. Polymers are applied both for providing food itself [6] and its packaging [7, 8]. Edible polymers can be added on the food surface to provide additional protection, and thus to keep products stable and maintain food quality. Furthermore, petroleum polymers can be used for packaging applications, which protect food from contaminants [9].

In addition, polymer films can be used as membranes as a results of their selective miscibility [10]. Also, they are used in electrical fields (e.g., dielectrics, insulators and safety hazards [11]). Polymers can be used in several other areas as well which demonstrates the reason behind their significance [12]. Discussing the details of each application is beyond the scope of this work.

In industry, we mostly deal with polymer blends in which two or more polymers are combined together to form a new material with tailored properties [13]. Blending polymers enables us to combine the desirable properties of several polymer components. Development of properties is also possible by designing new polymerization routes or new monomers. However, the two latter methods are usually more expensive and time consuming. Thus, the polymer blends are a cost effective option [14, 15]. In this work, we narrow our research to binary polymer blends.

When working with polymer blends, the importance of their surface properties is often critical. Many polymer blends applications, such as coatings, adhesives, and lubricants,

are dependent on the surface properties [16]. There can be significant differences between the bulk and surface properties, meaning that one component may segregate to the surface due to enthalpic or entropic reasons. Hence, a solid understanding of polymer surface properties is required for the above mentioned applications [17].

1.1 Polymerization

Now that we have discussed the importance of polymers in everyday life, the next few pages define some important terms in regard to polymer science. Polymers or macromolecules consist of a large number of molecular units that are connected by covalent bonds [18]. These molecular units are called monomers and are usually formed from carbon and hydrogen [19]. These monomers link together by a chemical reaction to form a polymer; this process is called polymerization [20, 21]. This concept is illustrated in figure 1.1. The number of monomers in each polymer molecule is called the degree of polymerization, which is denoted by N in this figure. If N is larger than 100, the molecule will be known as a polymer. There are some polymers with more than 10^5 monomers.

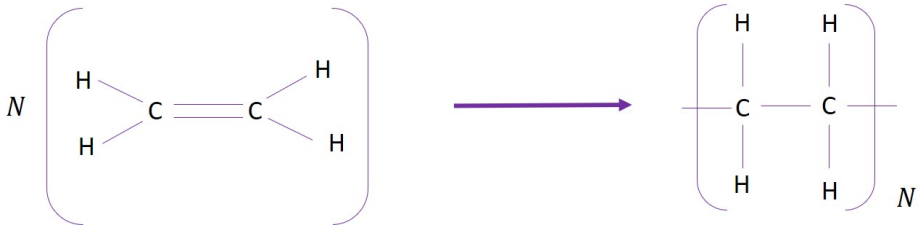

Figure 1.1: Polymerization

If identical monomers are linked together, the polymer is called a homopolymer. However, if two or more different monomers form a polymer chain, the polymer is called a copolymer. Copolymers can have different structures such as alternating copolymer, random copolymer, block copolymer and graft copolymer [22]. In this work, we focus on homopolymers and so we do not discuss copolymers any furthur.

1.2 Classifications of polymers

Polymers can be classified based on different aspects such as their origin, configuration, thermal properties, mechanical properties, etc. Blends generally involve polymers which

are different in one of the mentioned properties. Therefore, we provide a brief overview of different polymer classifications.

There are some polymers in nature such as RNA, DNA, proteins, which are called natural polymers. Some of the natural polymers even have more than 10^9 monomers [23]. In addition, semi-synthetic polymers are processed using natural polymers. For example, natural rubber is heated with sulfur to enhance its elastic properties. The other group of polymers is known as synthetic polymers like Teflon, nylon, polyester, and polyethylene [20].

Furthermore, polymers have different architectures. They can be linear, branched, or a cross-linked network. As shown in figure 1.2, linear polymers are long chains without any branches. These polymers are generally soluble in an appropriate solvent.

Branched polymers consist of a backbone with several small chains attached along its length. These branches may be formed from side reactions in the polymerization process. Branched polymers are more soluble than the linear ones since their intermolecular interactions are weaker. Cross-linked polymers form a three-dimensional network, which consists of numerous backbones joined together by covalent bonds [24].

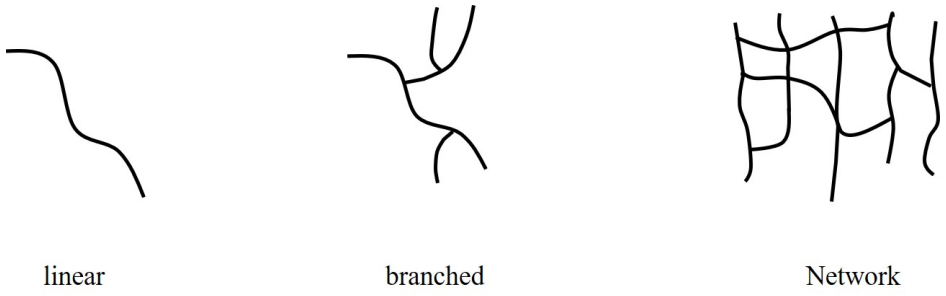

Figure 1.2: Polymer structures

The number of branches as well as their length affects the material properties. Polymers with different architecture have different surface energy, which leads to enrichment of the surface in one component rather than the other. The surface segregation of a binary polymer blend with a linear and a branched component has been a subject of several works which will be discussed in the literature review.

1.3 Polymer blends

Attaining knowledge about polymer blends is essential since they account for about 30% of plastics and this value increases annually (9% each year). Blending polymers is often done for several reasons such as increasing strength, improving processability and producing resistant, economic, and recyclable materials. When several different characteristics are needed, the most straightforward way to achieve them is to combine several polymers with different characteristics and produce a multi-component blend [25, 26].

In this work, our focus is on binary polymer blends, where two polymer components are blended to produce a novel material with new properties [25, 27]. A critical issue in blending is the miscibility of the components. Two components can be either miscible, immiscible or somewhere in the middle (i.e. partially miscible)[28]. Generally, two factors play role in miscibility of polymer blends; enthalpy and entropy, which will be elaborated on in the following lines.

It is known that negative enthalpy is one of the factors that helps the mixing to occur spontaneously. When two compounds are mixed, they can either absorb or release energy and generally mixing is more favorable if it releases energy. On the other hand, increasing the entropy of the system after mixing also contributes to the miscibility. This contribution is more significant in materials with low molecular weight. Take the example of a hexane-ethanol mixture, which is miscible due to the larger entropy, while polyolefins and poly(vinyl alcohol) are immiscible due to the smaller amount of entropy [28].

In order to check whether the two componets are miscible or not, the effect of entropy and enthalpy should be considered as well as the temperature. Note that in this section, for simplicity, the two components are the same in their size (degree of polymerization). The Gibbs free energy combines all these parameters as follows [13],

$$\Delta G_m = \Delta H_m - T\Delta S_m \tag{1.1}$$

where ΔG_m is the mixing free energy, ΔH_m is the mixing enthalpy, T is the temperature and ΔS_m is the mixing entropy. In order for two components to be miscible, ΔG_m needs to be negative [28].

Negative ΔG_m is a requirement for miscibility. However, that is not enough. There is another expression to be satisfied [15, 28].

$$\left(\frac{\partial^2 \Delta G_m}{\partial \phi_1^2}\right)_{T,P} > 0 \tag{1.2}$$

where ϕ_1 is the volume fraction of the first component and P shows the pressure. If the first condition (equation (1.1)) is satisfied and the second condition (equation (1.2)) is not, then the phase separation occurs, but not instantly [29, 1].

$$\frac{G_m}{nk_BT} = \phi_1 \ln \phi_1 + (1-\phi_1) \ln 1 - \phi_1 + \chi_N \phi_1 (1-\phi_1) \tag{1.3}$$

where k_B is the Boltzmann's constant and n is the total number of polymer molecules in the blend. The first two terms are the entropic contribution, while the third term is the enthalpic contribution to the mixing.

Here, χ is the interaction parameter, which is defined as [1, 30],

$$\chi \equiv \frac{2\epsilon_{12} - \epsilon_1 - \epsilon_2}{2k_BT\rho_0} \tag{1.4}$$

where ϵ_{12} is the interaction energy between the two polymer components, ϵ_1 and ϵ_2 are the interaction energies between like polymer molecules of the first and second component, respectively. ρ_0 is the segment density.

Generally, there are two kinds of entropy; one is due to the translational motion which is maximized when the polymer molecules are able to go everywhere and reduced by their restriction to certain domains. The first two terms on the left hand side of equation (1.3) correspond to traslational entropy. The maximum entropy occurs when the two components have equal probability to go everywhere ($\phi_1 = 0.5$). The other type of entropy is configurational entropy which is due to the polymer random walk. In a homogeneous blend, configurational entropy is unaffected by phase separation, since all the polymers do the random walk. Therefore, this entropy is not included in equation (1.3) [31].

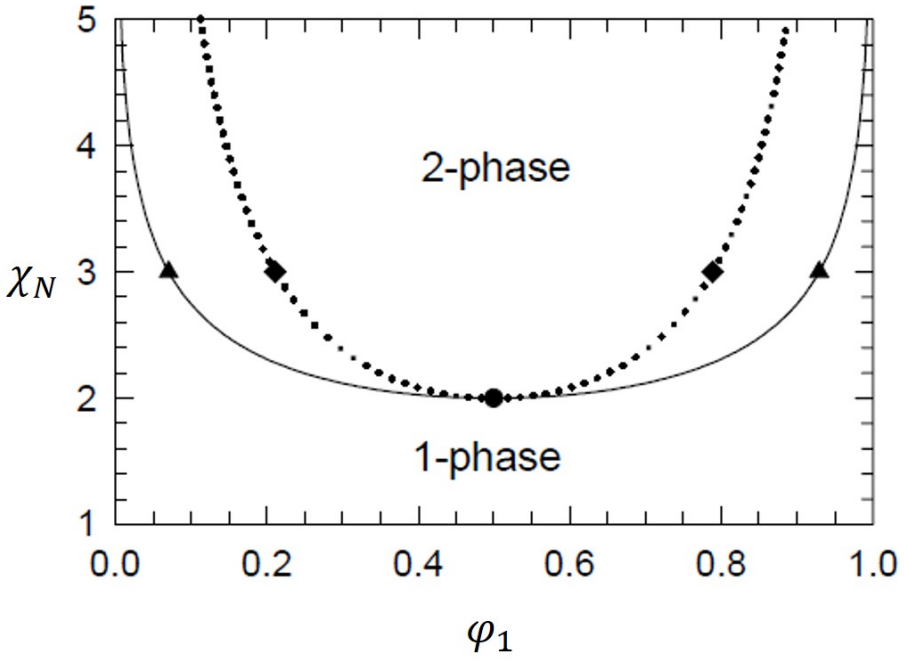

Figure 1.3: Phase diagram [1]

Figure 1.3 shows the phase diagram of a blend where both components have the same degree of polymerization, N. The dotted and the solid curves are the spinodal and binodal curves, respectively. Inside the spinodal curve, phase separation occurs quickly. In between the binodal and spinodal curve, phase seperation happens slowly by nucleation and growth. The binodal curve is the true phase boundary. χ is equal zero in this work. Hence, only entropic sources play role in polymer behavior that we are going to study in the following pages.

As one might expect, most polymer pairs are immiscible due to their high molecular weight, which in turn leads to low entropy. However, it is worth mentioning that the degree of compatibility can be widely different [13, 14]. As polymer blends are extremely practical materials, several works have been done to solve the miscibility issue and thus minimizing the mixing free energy [32, 33]. For example, addition of a third component which is compatible with both existing components is one of the methods which is applied for this issue [15].

1.4 Bulk properties

Here we use the freely jointed model to describe the configurations of polymers in the bulk. In this model, polymer units perform random walks, meaning that their trajectories are just a set of uncorrelated displacement [34, 35]. A lot of parameters, which are required for explaining polymer properties, are elaborated by using this model in the next few pages.

It is worth mentioning that a segment generally refers to a number of monomer units. However, the terms "segment" and "monomer" can be used interchangeably in the context of our work. In the next step, we wish to characterize the polymer size. There are several definitions that can be used for this purpose. In the following sections, we will discuss two of them.

1.4.1 End-to-end distance, R_0

In the freely jointed model, each polymer has $N-1$ bonds with length a along the chain, which can orient in any direction. Vector $\mathbf{r}_i$ points from the origin to the i^{th} monomer, and $\mathbf{u}_i$ points from the i^{th} monomer to $i+1^{th}$ monomer. Hence, we can say $\mathbf{u}_i = \mathbf{r}_{i+1} - \mathbf{r}_i$. As was mentioned before the segment length is a. Hence, it follows that $|\mathbf{u}_i| = a$ and $\langle \mathbf{u}_i \cdot \mathbf{u}_j \rangle = a^2 \delta_{ij}$ (where $<>$ is the ensemble average and δ_{ij} is the Kronecker delta function which is equal 1 for $i = j$, otherwise it is equal to zero.)

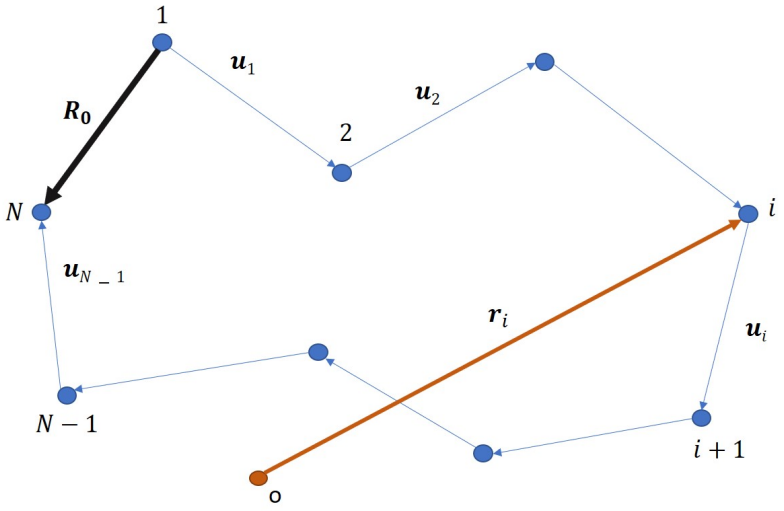

Figure 1.4: $\mathbf{r}_i$, $\mathbf{u}_i$ and $\mathbf{R_0}$ are shown in the figure.

The vector $\mathbf{R_0}$ points from the first monomer in the polymer chain to the last one. Hence, this vector can be expressed as

$$\mathbf{R_0} = \mathbf{r}_N - \mathbf{r}_1 = \sum_{i=1}^{N-1} \mathbf{r}_{i+1} - \mathbf{r}_i = \sum_{i=1}^{N-1} \mathbf{u_i} \tag{1.5}$$

By knowing the number of monomers along the polymer chain as well as the bond length, we have many different possibilities for $\mathbf{R_0}$. Hence, in order to attain a measure of its size, we calculate the root-mean-square (RMS) of $\mathbf{R_0}$ shown in figure 1.4. This parameter is called the average end-to-end length.

$$R_0^2 = \langle \mathbf{R_0} \cdot \mathbf{R_0} \rangle = \left\langle \sum_{i=1}^{N-1} \sum_{j=1}^{N-1} \mathbf{u_i} \cdot \mathbf{u_j} \right\rangle = a^2 \sum_{i=1}^{N-1} \sum_{j=1}^{N-1} \delta_{ij} = (N-1)a^2 \xrightarrow{\text{in the limit of large N}} R_0^2 \approx Na^2 \tag{1.6}$$

1.4.2 Radius of gyration, R_g

There is another quantity that is used to characterize the size of a polymer which is called radius of gyration, R_g [36]. For polymer melts, this quantity is proportional to square root of the degree of polymerization ($R_g \propto N^{0.5}$) [37].

The first step in deriving the radius of gyration is to define the center of mass. Consider a polymer chain with N monomers, each with the same mass. As mentioned before, the vector $\mathbf{r}_i$ points from origin to the each monomer. We also define the vector $\mathbf{r}_{CM}$, which points from the origin to the center of mass.

$$\mathbf{r}_{CM} = \frac{1}{N} \sum_{i=1}^{N} \mathbf{r}_i \tag{1.7}$$

To start, we draw a vector from the center of mass to each monomer along the polymer chain. These vectors are denoted by $\mathbf{d}_i = \mathbf{r}_i - \mathbf{r}_{CM}$.

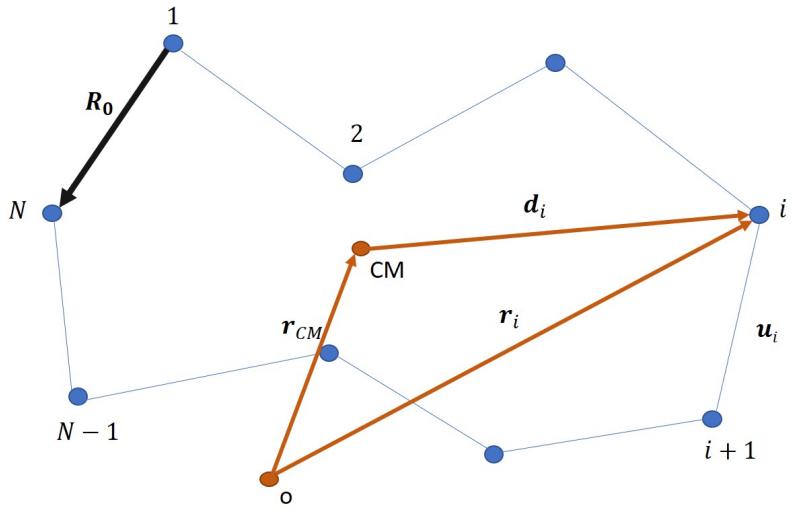

Figure 1.5: The center of mass as well as $\mathbf{r}_i$, $\mathbf{d}_i$ and $\mathbf{r}_{CM}$ are shown in the figure.

The radius of gyration is defined by the following equation,

$$R_g^2 = \frac{1}{N}\sum_{i=1}^{N}\left\langle |\mathbf{r}_i - \mathbf{r}_{CM}|^2 \right\rangle = \frac{1}{N}\sum_{i=1}^{N}\left\langle d_i^2 \right\rangle \tag{1.8}$$

To evaluate the sum in equation (1.8), we consider the following identity:

$$\begin{aligned}\sum_{i=1}^{N}\sum_{i=j}^{N}|\mathbf{d}_i - \mathbf{d}_j|^2 &= \sum_{i=1}^{N}\sum_{i=j}^{N}(d_i^2 - 2\mathbf{d}_i\cdot\mathbf{d}_j + d_j^2)\\ &= N\sum_{i=1}^{N}d_i^2 - 2\sum_{i=1}^{N}\sum_{j=1}^{N}\mathbf{d}_i\cdot\mathbf{d}_j + N\sum_{j=1}^{N}d_j^2\\ &= N\sum_{i=1}^{N}d_i^2 - 2\left[\sum_{i=1}^{N}\mathbf{d}_i\right]\cdot\left[\sum_{j=1}^{N}\mathbf{d}_j\right] + N\sum_{i=1}^{N}d_i^2\end{aligned} \tag{1.9}$$

It follows from the definitions of $\mathbf{d}_i$ and $\mathbf{r}_{CM}$ that $\sum_{i=1}^{N}\mathbf{d}_i = \sum_{i=1}^{N}(\mathbf{r}_i - \mathbf{r}_{CM}) = \sum_{i=1}^{N}\mathbf{r}_i -$

$N\mathbf{r}_{CM} = 0$. Furthermore, $\mathbf{r}_i - \mathbf{r}_j = \mathbf{d}_i - \mathbf{d}_j$ and therefore

$$\sum_{i=1}^{N}\sum_{i=j}^{N}\left\langle|\mathbf{r}_i - \mathbf{r}_j|^2\right\rangle = 2N\sum_{i=1}^{N}\left\langle d_i^2\right\rangle \tag{1.10}$$

Note that $\left\langle|\mathbf{r}_i - \mathbf{r}_j|^2\right\rangle$ is the end-to-end vector for a polymer chain which starts from the j^{th} monomer to the i^{th} one. Hence, this value is equal to $a^2|i-j|$ (where $|i-j|$ is the number of bonds between the i^{th} and j^{th} monomers. Thus, equation (1.8), can be written as follows,

$$R_g^2 = \frac{1}{2N^2}\left\langle|\mathbf{r}_i - \mathbf{r}_j|^2\right\rangle = \frac{a^2}{2N^2}\sum_{i=1}^{N}\sum_{j=1}^{N}|i-j| = \frac{a^2}{2N^2}\left(\sum_{i=1}^{N}\sum_{j=1}^{i-1}(i-j) + \sum_{i=1}^{N}\sum_{j=i+1}^{N}(j-i)\right) \tag{1.11}$$

By symmetry, the last two sums are equivalent and therefore $R_g^2 = \frac{a^2}{N^2}\sum_{i=1}^{N}\sum_{j=1}^{i-1}(i-j) = \frac{a^2}{N^2}\left(\sum_{i=1}^{N} i(i-1) - \sum_{i=1}^{N}\sum_{j=1}^{i-1} j\right)$. Using the fact that $\sum_{k=1}^{N} k = \frac{N(N+1)}{2}$, the second term can be simplified and thus $R_g^2 = \frac{a^2}{N^2}\left(\sum_{i=1}^{N} i(i-1) - \sum_{i=1}^{N}\frac{i(i-1)}{2}\right)$ and therefore $R_g^2 = \frac{a^2}{2N^2}\sum_{i=1}^{N} i(i-1) = \frac{a^2}{2N^2}\left(\sum_{i=1}^{N} i^2 - \sum_{i=1}^{N} i\right)$. Now, by the use of the fact that $\sum_{k=1}^{N} k^2 = \frac{N(N+1)(2N+1)}{6}$, we have $R_g^2 = \frac{a^2}{2N^2}\left(\frac{N(N+1)(2N+1)}{6} - \frac{N(N+1)}{2}\right)$. By simplifying, we have

$$R_g^2 = \frac{a^2 N}{6}\frac{N^2-1}{N^2} \approx \frac{a^2 N}{6} \tag{1.12}$$

Note that equation (1.12) is true when $N \gg 1$.

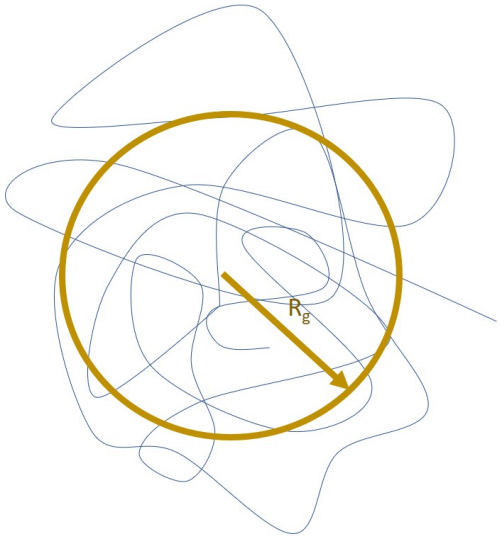

Figure 1.6: Radius of gyration

Figure 1.6 illustrates the radius of gyration of a single polymer chain. It should be mentioned that based on equations (1.6) and (1.12) the end-to-end distance and radius of gyration are proportional.

$$R_g = \frac{R_0}{\sqrt{6}} \tag{1.13}$$

Up to this point, two different quantities characteristic of the polymer size were introduced. In the next chapter, other quantities will be discussed in detail. In the following section, the focus is on the difference of the bulk and surface properties and the source of this difference.

1.5 Surface properties

Different polymer components are different both from entropic and enthalpic perspectives. This difference leads to the segregation of one component to the surface, which in turn leads to different compositions for the bulk and surface. For some applications, such as polymer processing, adhesion, and lubrication, it is essential to attain information about the properties of the polymer blend within a few angstroms of its surface [38].

Usually, the origin of segregation is mainly enthalpic. Generally, molecules do not prefer to be at the surface since they lose half of their interactions there. In the case of polymeric solutions, polymer molecules could stay in the bulk to benefit from their interactions. However, in the case of polymer blends, it would be a competition between different components to stay in the bulk and away from the surface [39].

In some cases, enthalpic differences may not be responsible for segregation and entropic sources lead to surface enrichment of polymer blends in one component. Generally, polymer molecules can move more freely in the bulk rather than the surface [40]. However, as we are dealing with polymer blends rather than polymer solutions, there will be a competition between two components for staying in the bulk. Various parameters will be responsible for the difference in entropic energies such as length, stiffness, configuration, etc.

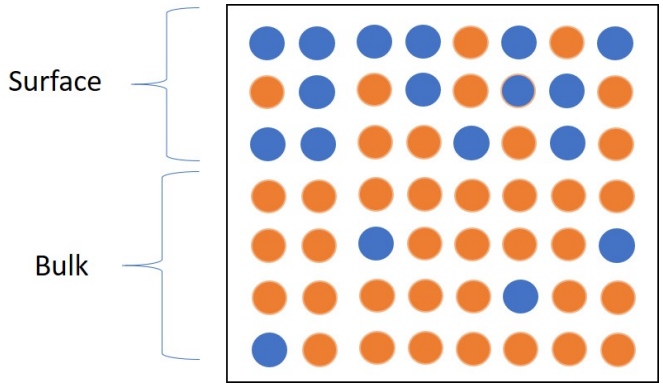

Figure 1.7: Polymer blend segregation. As the figure illustrates the blue component segregates to the surface and the bulk is richer in the orange ones.

The objective of this work is to study the effect of the different parameters on the segregation and find a universal behavior which enables us to have an estimation of the segregation before doing any complicated calculation.

1.6 Literature review

Nowadays, polymers play an essential role in many applications. In some of these applications, such as adhesion, coating, catalysis, membranes, lubrication, and polymer processing, attaining knowledge about surface structure and composition is crucial. Due to the entropic constraints at the surface, polymer molecules show different behavior at the

surface and in the bulk [41, 42]. Hence, the surface and bulk behavior should be studied individually. Nevertheless, the focus of this work is on surface properties.

In a binary polymer blend, the surface does not act as a reflecting boundary and it may be richer in one of the components. This surface enrichment affects some properties such as surface tension, wall slip, wettability, and the glass transition of thin films [43]. It is predicted that the segregation can be so significant that the surface is wetted only by one component [44]. It is worth mentioning that the surface itself affect the segregation behavior. For example, surface diffuseness has a considerable impact on the surface behavior meaning that the segregation is more significant when the surface is air rather than a hard substrate [45].

Predicting which component segregates to the surface has been the subject of a plethora of research projects recently. The segregation can be due to enthalpic or entropic forces. The difference in the interactions of the two polymers may cause surface enrichment in one component. Generally, if polymers segregate to the surface they lose half of their favorable interactions. Thus, generally, they do not prefer to be at the surface from an enthalpic point of view [39].

Considering enthalpic forces, in order to minimize the energy of the system, the surface should be enriched in the polymer component with the lower surface energy. As an example, if there are two different components in the blend and one of them is hydrophobic and the other is hydrophile, the former segregates to the surface. However, it is not always the component predicted from the enthalpic point of view that segregates to the surface, and entropic forces should be considered as a significant source that determines the segregation behavior [46].

Surface segregation due to entropic forces has been investigated from different perspectives such as segregation in the binary polymer blends due to disparity in size and rigidity. Each category attracts a lot of attention, which is elaborated in the following paragraphs [47, 48].

Generally, it is shown theoretically that the polymer component with a low degree of polymerization and a large number of ends segregates to the surface from an entropic point of view in a polydisperse polymer blend [49, 50]. Fleer et al. showed that surface segregation in polydisperse melts depends on the entropy loss of different components. For ideal chains, the entropy loss is proportional to the chain length i.e. the entropy loss for long chains is larger than short ones. Hence, the surface is enriched by the shorter polymer chains [50].

Surface enrichment in short polymer chains is also confirmed experimentally in other works. Bates et al. studied the surface segregation of polyolefin block copolymers using

poly(ethylene-propylene)-poly(ethyl ethylene) (PEP-PEE). No interaction was determined as discrimination between the two components. Deuteration was used to discriminate the blocks by neutron contrast. In all the cases, regardless of the surface (i.e. solid or air), the smaller block segregated to the surface [51].

However, the experimental methods, in which one of the components should be labeled by deuterium, such as neutron reflectivity (NR) [52, 53] and secondary ion mass spectrometry(SIMS) [54], cannot provide a reliable result since the labeling affects the segregation from the enthalpic point of view [55]. However, recently Hill et al. applied surface layer matrix assisted laser desorption ionization time-of-flight mass spectrometry (SL-MALDI-ToF-MS) to observe surface segregation based on length disparity in polymer blends. These experimental results confirmed that the shorter polymer component segregates to the surface [43].

Polymers generally have different levels of rigidity, which may affect the surface behavior as well. There are several works which investigated the surface segregation due to stiffness disparity. Wu et al. used the pure component parameter, $\beta^2 = \frac{Rg^2}{v_m}$, to characterize polymer flexibilities, where v_m is the molecular volume. This work shows that the component with a smaller value of β, i.e. the more flexible polymer component segregates to the surface due to entropic reasons [17]. This result is consistent with the work done by Fredrickson and Donley [56].

Kumar et al. introduced a bending potential to specify the stiffness of different polymer components. In this work, numerical wall polymer reference interaction site model (wall-PRISM) integral equation as well as the computer simulations were applied to show that in polymer blends the stiffer component segregates to the surface. It is stated that the reason behind this behavior is not only the local packing but also the local conformational changes [47]. Besides, by increasing stiffness disparity, density, and chain lengths, the segregation becomes more evident.

Stepanow and Fedorenko studied a polymer blend in which the two components were different in their statistical segment lengths near the hard wall by generalizing Edward's collective description. It is shown that stiffer polymers segregate to the surface [57].

In a work done by Yethiraj, it is shown that surface segregation is a function of density. This work predicts that for low-density polymers, the more flexible polymer segregates to the surface and in the liquid-like binary polymer blend, in which one component is stiffer than the other, the stiffer polymer segregates to the surface. Since the flexible polymers are less ordered, packing near the surface would be more challenging for them in comparison with the stiffer ones [58, 47].

As was mentioned above, there are different predictions for surface behavior due to

stiffness disparity based on the initial assumptions and the methods used for investigation. Hence, we should try to apply realistic and comprehensive assumptions and viable methods to get accurate results.

1.7 Motivation

In industry, we rarely deal with pure commercial plastics, and most materials are actually polymer blends [56]. This provides considerable motivation to study the behavior of polymer blends in detail. Furthermore, for many applications such as catalysis, membranes, corrosion, and biomaterials, we need to have some information about the surface properties [43]. Dealing with polymer blends, segregation behavior i.e., concentration profiles and structure, should be determined [51].

Some experimental methods need to label one polymer component, such as neutron reflectivity (NR) [52, 53] and secondary ion mass spectrometry(SIMS)[54]. Although, deuterium labeling is not the best way for monitoring the segregation due to the entropic sources, as it may create enthalpic interactions which may in turn affect the results [55].

Recently, SL-MALDI-TOF-MS method has been used to study the surface segregation behavior for a polymer blend where the components are different in their lengths [43]. So far, there is no acceptable experimental method to study the surface enrichment when the two polymer components are different in their stiffness. Until a valid experimental method is found, there is no option other than studying the surface segregation by the use of theory and simulation.

Going through different works in this area, we can see that there is lack of general understanding regarding which component segregates to the surface due to stiffness disparity [51, 58, 47, 56], which was the motivation for us to study this topic.

1.8 Thesis outline

In this work, the surface composition of a 50-50 binary polymer blend is studied. Two polymers have identical interactions and the same molecular volume meaning that $v_m = a_m \ell_c$, where a_m is the cross-sectional area and ℓ_c is the contour length of the chain. Thus, if they are longer they should be also thinner and if they are shorter they should be also thicker. Although, two polymer components are different in their conformational properties e.g., end-to-end, contour and persistence lengths.

In this thesis, initially, the Gaussian chain model and the worm-like chain model are introduced and the diffusion equation is solved for each case to attain the recursion relation for the partial partition function. Next, the single-chain partition function, concentration, excess concentration, and integrated excess are derived.

We wish to predict the surface composition at the surface and compare the two models. Using Gaussian chain model, one of the main assumptions is that the polymer chain is totally flexible. However, this assumptions is not realistic for many polymer chains as they have some level of rigidity. As the polymer chain become longer and their molecular weight increases, this model works better. In this model, the only parameter is the end-to-end distance of the two polymer components.

On the other hand, we work with the worm-like chain model in which we have more realistic assumptions and thus, the results are more precise. However, the calculation for this model is more complicated and time consuming in respect with the Gaussian chain model. In this model, we have two parameters; contour length and persistence length of the two polymer components. In this model, we can quantify the rigidity of both polymer components. The significance of this model is that we can study the surface segregation of a binary polymer blend in which one of the components is stiffer than the other. For the worm-like chain model, three different cases are considered; different contour lengths, different persistence lengths, and the same end-to-end distance with different individual values for contour and persistence lengths.

Finally, in the result section, the excess concentration profiles for the two components with different conformational properties are presented for the Gaussian chain as well as the worm-like chain model. In addition, the universal behavior is studied. The excess concentration profiles could be collapsed under appropriate conditions, which is called universal behavior. The significance of universal behavior is that we can have an estimation of the peak height and integrated excess of the excess concentration profiles of a binary polymer blend with a simple calculation.

Chapter 2

Modeling

In this chapter, several common models are introduced. Specifically, the Gaussian chain and worm-like chain models are discussed in detail as they are used to represent polymer chains in this work. This thesis aims to predict the concentration of binary polymer blends at the surface, where the concentration in the bulk is 50-50, and quantify the segregation.

The two polymer components have identical interactions and the same molecular volume (i.e. the one which is shorter is thicker and the one which is longer is thinner). It is worth mentioning that as the two polymer components are similar in their interactions, the surface segregation can not be due to enthalpic forces and thus entropic forces are responsible for this surface enrichment in one component. The system is solved in a canonical ensemble.

2.1 Self-consistent field theory (SCFT)

Generally, working with large molecules such as polymers is easier than working with small molecules such as water. Polymer molecules, typically have 10^3 to 10^5 monomers and this large number of monomers reduces the effect of monomer type on the polymer properties. It is worth mentioning that as polymer chains are highly interdigitated, one polymer may be in contact with a plethora of other polymer chains. Considering all these interactions, our calculation could be extremely complicated.

Simulating equilibrium behavior of polymeric systems would be possible by the application of molecular dynamics (MD) and Monte Carlo (MC) simulations. Although, there is another powerful approach, known as self-consistent field theory, which is a statistical

mechanics tool [3]. By applying this approach, instead of considering all inter-chain interactions among polymer chains, we just consider one polymer but in an external field [1] (i.e. the field represents the non-bonded interactions among monomers [59]). Thus, SCFT [60, 61] enables us to convert a fully interacting system to a single polymer in an external field. The partition function can be obtained by solving a diffusion equation.

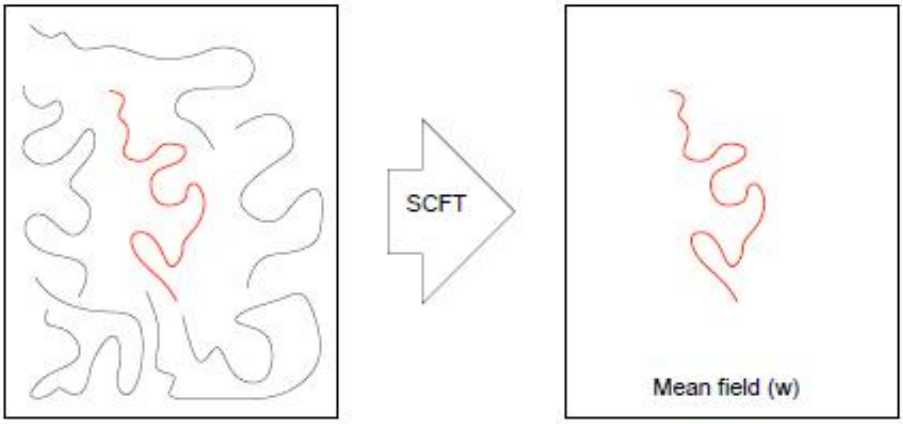

Figure 2.1: Self-consistent field theory

Concentration should have a sigmoidal profile, which is given as

$$\phi_{\text{ref}}(z) = \frac{1}{2}(1 + \tanh(\frac{2z}{\xi})) \tag{2.1}$$

where ξ is the width of the surface and z is the distance from the surface. All the lengths will be scaled with respect to ξ. The reference concentration is shown in the figure 2.2.

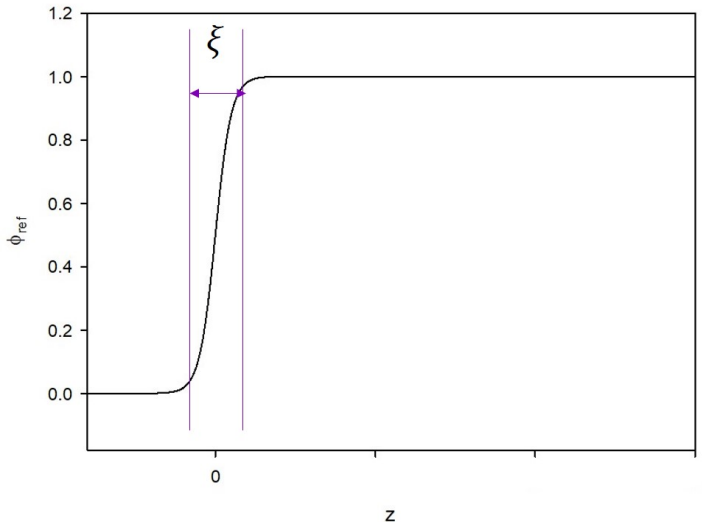

Figure 2.2: Sigmoidal shape of reference concentration

The next step is to determine the external field in a way that all the interactions among polymer chains can be substituted by it. In order to do so, we adjust the field in a way to attain this sigmoidal profile for the reference concentration, $\phi_{\text{ref}}(z)$ [59].

To determine the field, we use the simple and Anderson mixing algorithms, which are discussed at the end of this chapter. After determining the field, the next step is to decide about the best model to use in the work. This decision depends on the polymer characteristics that we wish to represent (e.g. stiffness, length, etc.).

Now, we move on to the next step, which is determining an appropriate model for representing the polymer chains. Initially, different models are brought up and after that, the models which will be used in this work are illustrated. There are different models, such as the rigid rod [62, 63, 64], the freely jointed model [65, 66, 67], the bead-spring model [68, 69, 70], the Gaussian chain model [71, 72, 73] and the worm-like chain model [74, 75, 76].

The rigid rod model considers polymers to be thoroughly rigid. This model could be used for modeling liquid crystalline molecules [77]. Usually, polymers have some level of flexibility (specially as they get longer). Thus, this model is not the best model to use as it does not take flexibility into account.

In the freely jointed model, there are several rigid rods connected with totally flexible bonds. This model could be used to model nucleic acid and proteins. In this model,

monomers do not have orientational interactions with each other and it can be mostly used for understanding physics of polymers. The bond angle can change freely but the distance between two units is constant. Here we encounter the concept of random walks for polymer configurations. This means that the bond can have any angle and the beads can have any position. The characteristic size of the polymer configuration is given by the average end-to-end distance, R_0. It should be taken into account that the random walk can not describe polymer behavior, which is the limitation of this model.

Next model is the bead-spring model, where instead of rigid rods in the freely jointed model, we substitute springs. This model contains $N+1$ beads, which are made of several repeat subunits, connected by N springs.

In addition to these three models, there are the Gaussian and worm-like chain models. In the Gaussian chain model, we assume that the polymer chain is completely flexible. Hence, there is no orientation in this model. All the polymers have some level of rigidity. However, when the polymer gets longer, their rigidity becomes less significant. Thus, this model could be used for long flexible polymer chains.

At the end, there is the worm-like chain model, which assumes some level of rigidity for the polymer chain. This model represents polymer chains more realistically, but its calculations are more complicated than the Gaussian chain model. In this work, the Gaussian and worm-like chain models are used to study polymer blend segregation. Therefore, these two models are elaborated in detail in the following pages.

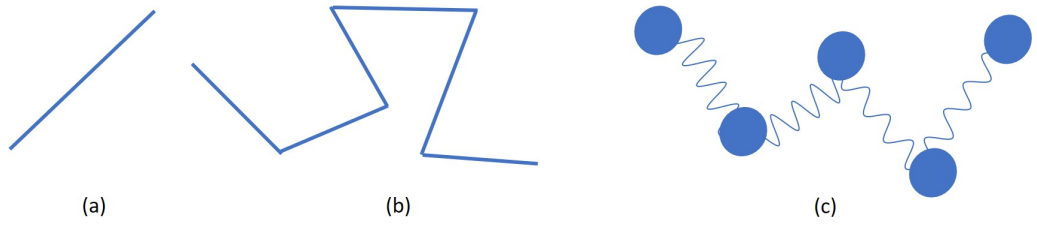

Figure 2.3: (a) Rigid rod (b) Freely jointed chain (c) Bead-spring model

2.2 Gaussian chain model

The Gaussian chain is a convenient model for analytical and numerical calculations. However, each model has several assumptions which should be satisfied in order to have validate results. In this model, it is assumed that the polymer chain is completely flexible, which is

true only for long chains with a high molecular weight. The smallest length in this model is the segment length which is denoted by a.

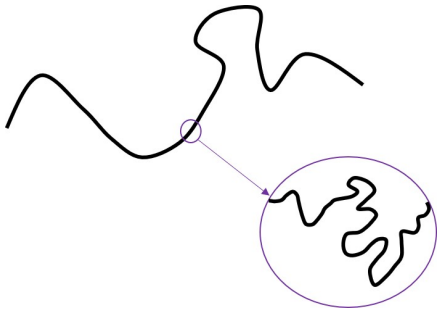

Figure 2.4: Gaussian chain model

In the following pages, partial partition functions are obtained. After that, the single-chain partition function and concentration of each component are calculated [78, 1]. The only parameter in this model is end-to-end distance, R_0, of two polymers, which was discussed in the previous chapter.

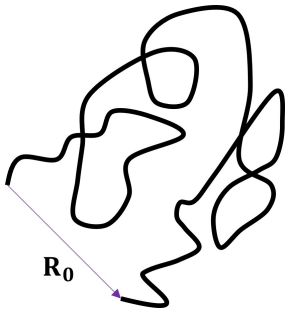

Figure 2.5: End-to-end distance

In the following pages, the partial partition function, q(z,s), is being calculated, where s=0 to 1 is a contour variable along the length of polymer. In order to do so, we need the initial condition and recursion relation.

$$q(z, 0) = 1 \tag{2.2}$$

For solving the recursion relation, one can use the Crank-Nicolson method [79]. q(z,s)

satisfies the diffusion equation below

$$\frac{\partial q(z,s)}{\partial s} - \alpha^2 \frac{\partial^2 q(z,s)}{\partial^2 z} + w(z)q(z,s) = 0, \quad 0 < z < D,\ 0 < s < 1 \tag{2.3}$$

where $\alpha^2 = \frac{R_0^2}{6}$ and s is the backbone parameter and D is the box size. We have Neumann boundary condition at both ends. Also, the initial condition was given in equation (2.2).

We discretize equation (2.3) by defining $i = s$, $i+1 = s+\Delta s$, $j = z$ and $j+1 = z+\Delta z$. Applying the forward-difference method at ith step in the diffusion equation, we have

$$\frac{q^{i+1,j} - q^{i,j}}{\Delta s} - \alpha^2 \frac{q^{i,j+1} - 2q^{i,j} + q^{i,j-1}}{\Delta z^2} + w^i q^{i,j} = 0 \tag{2.4}$$

Similarly, for the backward-difference method at $(i+1)$st step we have

$$\frac{q^{i+1,j} - q^{i,j}}{\Delta s} - \alpha^2 \frac{q^{i+1,j+1} - 2q^{i+1,j} + q^{i+1,j-1}}{\Delta z^2} + w^{i+1} q^{i+1,j} = 0 \tag{2.5}$$

by the use of equation (2.4) and (2.5) one can apply the averaged-difference method.

$$\begin{aligned} &\frac{q^{i+1,j} - q^{i,j}}{\Delta s} - \frac{\alpha^2}{2} \frac{q^{i,j+1} - 2q^{i,j} + q^{i,j-1}}{\Delta z^2} + \frac{1}{2} w^i q^{i,j} \\ &- \frac{\alpha^2}{2} \frac{q^{i+1,j+1} - 2q^{i+1,j} + q^{i+1,j-1}}{\Delta z^2} + \frac{1}{2} w^{i+1} q^{i+1,j} = 0 \end{aligned} \tag{2.6}$$

Equation (2.6) can be reexpressed in matrix form in which the column vectors $q^{(i+1)}$ and $q^{(i)}$ are related by

$$Aq^{(i+1)} = Bq^{(i)} \quad i = 0, 1, 2, ... \tag{2.7}$$

where A and B are matrices. In order to define these two matrices, we should rewrite equation (2.6). For simplicity, we define $\lambda = \frac{\alpha^2 \Delta s}{\Delta z^2}$ and substitute it.

$$\begin{aligned} q^{i+1,j} - q^{i,j} - \frac{\lambda}{2} \left[q^{i,j+1} - 2q^{i,j} + q^{i,j-1} + q^{i+1,j+1} - 2q^{i+1,j} + q^{i+1,j-1} \right] \\ + \frac{\Delta s}{2} (w^i q^{i,j} + w^{i+1} q^{i+1,j}) = 0 \end{aligned} \tag{2.8}$$

Now, by writing equation (2.8) in the form of equation (2.7), we obtain

$$-\frac{\lambda}{2}q^{i+1,j-1}+(1+\lambda+\frac{\Delta s}{2}w^{i+1})q^{i+1,j}-\frac{\lambda}{2}q^{i+1,j+1}= \\ \frac{\lambda}{2}q^{i,j-1}+(1-\lambda-\frac{\Delta s}{2}w^{i})q^{i,j}+\frac{\lambda}{2}q^{i,j+1} \tag{2.9}$$

In the next step, A and B can be written in this way;

$$A=\begin{pmatrix} 1+\lambda+\frac{w^1\Delta S}{2} & -\lambda & 0 & \cdots & 0 \\ -\frac{\lambda}{2} & 1+\lambda+\frac{w^2\Delta S}{2} & -\frac{\lambda}{2} & \ddots & \vdots \\ 0 & & & & \vdots \\ \vdots & \ddots & \ddots & \ddots & 0 \\ \vdots & \ddots & -\frac{\lambda}{2} & 1+\lambda+\frac{w^{n-1}\Delta S}{2} & -\frac{\lambda}{2} \\ 0 & \cdots & 0 & -\lambda & 1+\lambda+\frac{w^n\Delta S}{2} \end{pmatrix}$$

$$B=\begin{pmatrix} 1-\lambda-\frac{w^1\Delta S}{2} & \lambda & 0 & \cdots & 0 \\ \frac{\lambda}{2} & 1-\lambda-\frac{w^2\Delta S}{2} & \frac{\lambda}{2} & \ddots & \vdots \\ 0 & & & & \vdots \\ \vdots & \ddots & \ddots & \ddots & 0 \\ \vdots & \ddots & \frac{\lambda}{2} & 1-\lambda-\frac{w^{n-1}\Delta S}{2} & \frac{\lambda}{2} \\ 0 & \cdots & 0 & \lambda & 1-\lambda-\frac{w^n\Delta S}{2} \end{pmatrix}$$

The single partition function for the i^{th} polymer type is

$$Q_i=\int dz q_i(z,s)q_i(z,1-s) \tag{2.10}$$

where i can be either 1 or 2. By the application of statistical mechanics, we obtain

$$\phi_i(z)\propto\int_0^1 ds q_i(z,s)q_i(z,1-s) \tag{2.11}$$

for the concentration of component i.

In order to convert the proportional sign to equal, one shall insert a constant k.

$$\phi_i(z) = k \int_0^1 ds q_i(z,s) q_i(z,1-s) \tag{2.12}$$

To determine k, we integrate over z.

$$\int \phi_i(z) dz = k \int_0^1 ds \int dz q_i(z,s) q_i(z,1-s) \tag{2.13}$$

By applying equation (2.10) we have

$$\frac{n_i}{n} D = k Q_i \tag{2.14}$$

where n_i is the number of polymer chains of component i and $n = n_1 + n_2$ is the total number of polymer chains in the blend. Based on equation (2.14), the constant could be calculated and substituted in equation (2.12) to obtain

$$\phi_i(z) = \frac{n_i D}{n Q_i} \int_0^1 ds q_i(z,s) q(z,1-s) \tag{2.15}$$

There are two important parameters in this regard; excess concentration and integrated excess. Excess concentration is defined as follows,

$$\delta\phi_i(z) = \phi_i(z) - \bar{\phi}_i \phi_{ref}(z) \tag{2.16}$$

where $\bar{\phi}_i$ is the bulk concentration for component i. The integrated excess is defined by

$$\frac{\Theta_{ex,i}}{\rho_0} = \int \delta\phi_i(z) dz \tag{2.17}$$

where ρ_0^{-1} is the volume of an individual segment.

The Gaussian chain model is popular because of its easy formulation. However, it has some limitations. The Gaussian chain model assumes that polymer chains are long and flexible, and thus it can not explain some of the physical properties that are associated with the discreteness of chains. Some examples can be found in [3]. If we are dealing with short polymer chains or stiff ones, using the worm-like chain model would be recommended, which is illustrated in the following pages.

2.3 Worm-like chain model

The worm-like chain model, unlike the Gaussian chain model, includes the energy cost associated with bending. In the worm-like chain model, we consider orientation dependence, as well as backbone parameter and distance from the surface. Using the worm-like chain model for representing the polymer chain makes the calculations more complicated since we consider the orientation variable all along the polymer chain.

In the Gaussian chain model, only the energy associated with local stretching is considered. However, for the worm-like chain model in addition to that the energy of local bending is considered, which makes the predictions more realistic. The parameter κ controls the bending rigidity. The smallest length in this model is the segment bond length ,b, and each polymer has N segments along the chain.

The contour length (l_c) and persistence length (l_p) of each polymer component represent the parameters in this model. Contour length is the length of the polymer chain when it is stretched out and persistence length is the typical distance over which the orientation remains relatively constant. If persistence length is much smaller than the contour length, the polymer chain becomes flexible and approaches the Gaussian chain limit. If persistence length is considerable with respect to the contour length, then the polymer chain approaches a rigid rod. The chain contour length and persistence length can be represented using the parameters mentioned earlier, $l_c = Nb$ and $l_p = \kappa b$.

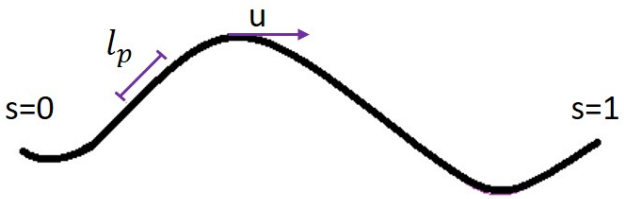

Figure 2.6: The worm-like chain model

Figure 2.6 shows a polymer chain, represented by the worm-like chain model, where $\mathbf{u}(s)$ is a unit tangent vector, which gives the orientation at each point. Furthermore, $\mathbf{r}(s)$ is the position vector, which starts from the origin and ends at the point associated with s on the polymer chain. Thus, the vector $\mathbf{R}$, defining the end-to-end distance, is equal to $\mathbf{r}(1) - \mathbf{r}(0)$. It should be emphasized that s, which is the backbone parameter, should be in the range of $[0, 1]$. Now, that all the other parameters are determined, one can define

the unit tangent vector as follows,

$$\mathbf{u}(s) \equiv \frac{1}{bN}\frac{d}{ds}\mathbf{r}(s) \tag{2.18}$$

Generally, one could change contour and persistence length of two components as well as the width of the surface to study their effects. In this work, our variables are $\frac{l_c}{\xi}$ and $\frac{l_p}{\xi}$ for both polymer components. The end-to-end distance of the worm-like chain can be expressed in terms of the contour and persistence lengths by equation (2.19)[80].

$$R_0 = \sqrt{2l_p l_c}\sqrt{(1 - \frac{l_p}{l_c}[1 - \exp(-\frac{l_c}{l_p})])} \tag{2.19}$$

The second term is a correction factor. For long chains, where $l_c \gg l_p$, this formula simplifies to

$$R_0 = \sqrt{2l_c l_p} \tag{2.20}$$

As implied by equation (2.20), a polymer with a large persistence length (i.e. a stiff polymer chain) and a polymer with a large contour length (i.e. long polymer chain) will tend to have a large end-to-end distance.

Now, as we did for the Gaussian chain model, we derive a recursion relation for partial partition function. With this in mind, we can extend the partition function in terms of Legendre polynomials and substitute it in the diffusion equation. The diffusion equation is as follows [80, 81, 82],

$$\frac{\partial q(\mathbf{r},\mathbf{u},s)}{\partial s} + l_c\mathbf{u}\cdot\nabla_r q(\mathbf{r},\mathbf{u},s) = \frac{l_c}{2l_p}\nabla^2_{\mathbf{u}} q(\mathbf{r},\mathbf{u},s) - w(\mathbf{r},\mathbf{u})q(\mathbf{r},\mathbf{u},s) \tag{2.21}$$

It is worth mentioning, that the reverse partition function, $q^\dagger(\mathbf{r},\mathbf{u},s)$ satisfies the same equation with one hand side multiplied by -1 [81]. We know that $q^\dagger(\mathbf{r},\mathbf{u},s)$ is equal $q(\mathbf{r},-\mathbf{u},1-s)$. In this work, we tend to solve the equation in one dimension. Thus, $\mathbf{r}$ can be replaced by z and $\mathbf{u}$ can be replaced by u_z giving

$$\partial_s q(z,u_z,s) + l_c u_z \partial_z q(z,u_z,s) = \frac{l_c}{2l_p}\nabla^2_{u_z} q(z,u_z,s) - w(z)q(z,u_z,s) \tag{2.22}$$

where $u_z = \cos(\theta)$ is expressed in terms of θ, which is the angle relative to the z axis. In

this work, the field does not have θ dependence, We can expand the partition function in terms of Legendre polynomials, but before that, we have to know some basic mathematics regarding functional expansions [83, 84, 85].

2.3.1 Orthogonal basis functions

We can expand a vector in three dimensional space into its components, as an example the vector shown in figure 2.7 could be written in this way;

$$\vec{\mathbf{M}} = M_x\hat{\mathbf{i}} + M_y\hat{\mathbf{j}} + M_z\hat{\mathbf{k}} \tag{2.23}$$

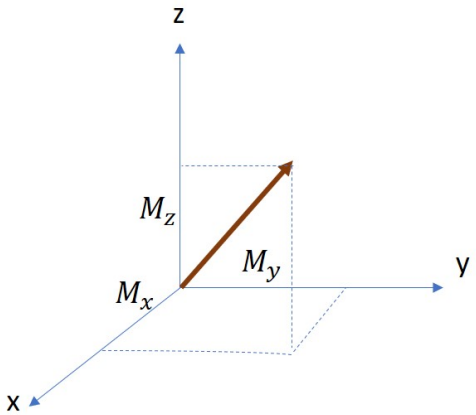

Figure 2.7: Orthogonal functions

where M_x, M_y and M_z are components, $\hat{\mathbf{i}}$, $\hat{\mathbf{j}}$ and $\hat{\mathbf{k}}$ are orthogonal basis functions meaning that the inner product of any two of them is equal to zero.

$$\hat{\mathbf{i}} \cdot \hat{\mathbf{j}} = \hat{\mathbf{i}} \cdot \hat{\mathbf{k}} = \hat{\mathbf{j}} \cdot \hat{\mathbf{k}} = 0 \tag{2.24}$$

Now, for calculating M_x, we have

$$\vec{\mathbf{M}} \cdot \hat{\mathbf{i}} = M_x\hat{\mathbf{i}} \cdot \hat{\mathbf{i}} + M_y\hat{\mathbf{j}} \cdot \hat{\mathbf{i}} + M_z\hat{\mathbf{k}} \cdot \hat{\mathbf{i}} \tag{2.25}$$

$$M_x = \frac{\vec{\mathbf{M}} \cdot \hat{\mathbf{i}}}{\hat{\mathbf{i}} \cdot \hat{\mathbf{i}}} = \frac{\vec{\mathbf{M}} \cdot \hat{\mathbf{i}}}{\left|\hat{\mathbf{i}}\right|^2} \tag{2.26}$$

where $\left|\hat{\mathbf{i}}\right|$ denotes the magnitude of vector $\hat{\mathbf{i}}$. These basis functions are normalized, and so this value is equal to one. The similar steps can be taken to calculate M_y and M_z. In the above discussion, we used the inner product of two vectors $(\mathbf{u}, \mathbf{v})$, which has the following properties;

$$\begin{aligned} (\mathbf{u}, \mathbf{v}) &= (\mathbf{v}, \mathbf{u}) \\ (k\mathbf{u}, \mathbf{v}) = (\mathbf{v}, k\mathbf{u}) &= k(\mathbf{u}, \mathbf{v}) \\ (\mathbf{u}, \mathbf{u}) &\geq 0 \\ (\mathbf{u} + \mathbf{w}, \mathbf{v}) &= (\mathbf{u}, \mathbf{v}) + (\mathbf{w}, \mathbf{v}) \end{aligned} \tag{2.27}$$

In this part, we define the inner product for two functions instead of two vectors as [84]

$$(f_1, f_2) = \int_a^b f_1(x) f_2(x) dx \tag{2.28}$$

where f_1 and f_2 are two functions defined on the interval $[a, b]$. If the inner product of these two functions is equal to zero, they are said to be orthogonal. Although, in this area one important point should be considered. When two vectors are orthogonal, it means that they are perpendicular, but this is not true for functions. Two functions being orthogonal does not have any geometric significance [83, 86].

2.3.2 Legendre polynomials

The Legendre polynomial $P_l(x)$ represents a bounded solution for a second-order differential equation [87]. $P_l(x)$ can be defined as follows,

$$P_l(x) = \frac{1}{2^l l!} \frac{d^l}{dx^l} (x^2 - 1)^l \quad l \geq 0 \tag{2.29}$$

We can expand any function in terms of Legendre polynomials in this way,

$$f(x) = \sum_{l=0}^{\infty} C_l P_l(x) \tag{2.30}$$

where C_l can be defined based on following equation,

$$C_l = \frac{1}{||P_l||^2} \int_{-1}^{1} P_l(x) f(x) dx \tag{2.31}$$

One can show that

$$||P_l||^2 = (P_l, P_l) = \int_{-1}^{1} P_l^2(x) dx = \frac{2}{2l+1} \tag{2.32}$$

Here are first few Legendre polynomials which can be calculated by applying equation (2.29) [88],

$$P_0(x) = 1 \tag{2.33a}$$
$$P_1(x) = x \tag{2.33b}$$
$$P_2(x) = \frac{1}{2}(3x^2 - 1) \tag{2.33c}$$
$$P_3(x) = \frac{1}{2}(5x^3 - 3x) \tag{2.33d}$$
$$P_4(x) = \frac{1}{8}(35x^4 - 30x^2 + 3) \tag{2.33e}$$
$$P_5(x) = \frac{1}{8}(63x^5 - 70x^3 + 15x) \tag{2.33f}$$

Legendre polynomials are orthogonal over $(-1, 1)$, which could be shown as follows,

$$\int_{-1}^{1} P_l(u) P_{l'}(u) du = \frac{2}{2l+1} \delta_{ll'} \tag{2.34}$$

where $\delta_{ll'}$ is the Kronecker delta function. This equation means that if $l \neq l'$ the result is zero, otherwise, it is $\frac{2}{2l+1}$.

Other properties of Legendre polynomials are shown in the following equations,

$$\nabla_u^2 P_l(u) = -l(l+1) P_l(u) \tag{2.35}$$

$$\int P_l(u) P_{l'}(u) P_{l''}(u) du = 2\Gamma^2_{l,l',l''} \tag{2.36}$$

In the case that the sum of l, l' and l'' is even and $|l-l'| \leq l'' \leq l+l'$, then

$$\Gamma^2_{l,l',l''} = (-1)^k \sqrt{\frac{(2k-2l)!(2k-2l')!(2k-2l'')!}{(2k+1)!}} \frac{k!}{(k-l)!(k-l')!(k-l'')!} \tag{2.37}$$

and otherwise, $\Gamma_{l,l',l''} = 0$. In equation (2.37), k is equal to $\frac{l+l'+l''}{2}$.

In order to solve the equation, we can expand the partition function in terms of Legendre polynomials and substitute that into the diffusion equation.

$$q(z, u_z, s) = \sum_l q_l(z, s) P_l(u_z) \tag{2.38}$$

2.3.3 Taylor series expansions

Initial value partial differential equations are solved numerically by the use of a Taylor series expansion [89, 90]. Expanding $q(z, u_z, s + \Delta s)$, we have

$$\begin{aligned} q(z, u_z, s+\Delta s) = q(z, u_z, s) + \Delta s \partial_s q(z, u_z, s) + \frac{(\Delta s)^2}{2!} \partial_s^2 q(z, u_z, s) + \\ \frac{(\Delta s)^3}{3!} \partial_s^3 q(z, u_z, s) + \frac{(\Delta s)^4}{4!} \partial_s^4 q(z, u_z, s) + O(\Delta s^5) \end{aligned} \tag{2.39}$$

For simplification, we can just keep the first three terms on the right hand side of equation (2.39) and neglect the other terms as they are so small. By moving $q(z, u_z, s)$ to the left hand side of the equation and dividing by Δs we have

$$D_s \equiv \frac{q(z, u_z, s+\Delta s) - q(z, u_z, s)}{\Delta s} = \partial_s q(z, u_z, s) + \frac{\Delta s}{2!} \partial_s^2 q(z, u_z, s) + O(\Delta s^2) \tag{2.40}$$

Similarly, the expansion for $q(z + \Delta z, u_z, s)$ is

$$\begin{aligned} q(z+\Delta z, u_z, s) = q(z, u_z, s) + \Delta z \partial_z q(z, u_z, s) + \frac{(\Delta z)^2}{2!} \partial_z^2 q(z, u_z, s) + \\ \frac{(\Delta z)^3}{3!} \partial_z{}^3 q(z, u_z, s) + \frac{(\Delta z)^4}{4!} \partial_z^4 q(z, u_z, s) + O(\Delta z^5) \end{aligned} \tag{2.41}$$

Subtracting the analogous expansion for $q(z-\Delta z, u_z, s)$ obtained by switching the sign of Δz, we obtain

$$\begin{gathered} q(z+\Delta z, u_z, s) - q(z-\Delta z, u_z, s) = 2\Delta z \partial_z q(z, u_z, s) + \\ 2\frac{(\Delta z)^3}{3!}\partial_z{}^3 q(z, u_z, s) + 2\frac{(\Delta z)^5}{5!}\partial_z^5 q(z, u_z, s) + O(\Delta z^7) \end{gathered} \tag{2.42}$$

Similarly, by dividing equation (2.42) by $2\Delta z$ we have,

$$D_z \equiv \frac{q(z+\Delta z, u_z, s) - q(z-\Delta z, u_z, s)}{2\Delta z} = \partial_z q(z, u_z, s) + \frac{(\Delta z)^2}{3!}\partial_z^3 q(z, u_z, s) + O(\Delta z^4) \tag{2.43}$$

For obtaining D_{zz}, we have to write D_z once base on the difference between $q(z+\Delta z, u_z, s)$ and $q(z, u_z, s)$ and the other time between $q(z, u_z, s)$ and $q(z-\Delta z, u_z, s)$. The other steps can be written as follows,

$$\begin{gathered} D_{zz} \equiv \frac{q(z+\Delta z, u_z, s) - 2q(z, u_z, s) + q(z-\Delta z, u_z, s)}{\Delta z^2} = \\ \partial_z^2 q(z, u_z, s) + 2\frac{(\Delta z)^2}{4!}\partial_z^4 q(z, u_z, s) + 2\frac{(\Delta z)^4}{6!}\partial_z^6 q(z, u_z, s) + O(\Delta z^6) \end{gathered} \tag{2.44}$$

2.3.4 Solving the equations

Now, we can write equation (2.22) by the help of Legendre polynomials in this way,

$$\begin{gathered} P_l(u_z)\partial_s q_l(z, s) + l_c u_z P_l(u_z)\partial_z q_l(z, s) = \\ \frac{l_c}{2l_p}\nabla_{u_z}^2 P_l(u_z) q_l(z, s) - w(z) q_l(z, s) P_l(u_z) \end{gathered} \tag{2.45}$$

As it can be understood from equation (2.33b), $P_1(\cos\theta) = \cos\theta = u_z$, so we can substitute u_z in equation (2.45) with $P_1(u_z)$. In addition, by the use of equation (2.35), we can substitute $\nabla_{u_z}^2 P_l = -l(l+1)P_l$ giving

$$\begin{gathered} P_l(u_z)\partial_s q_l(z, s) + l_c P_1(u_z) P_l(u_z)\partial_z q_l(z, s) = \\ -\frac{l_c}{2l_p} l(l+1) P_l(u_z) q_l(z, s) - w(z) q_l(z, s) P_l(u_z) \end{gathered} \tag{2.46}$$

If we multiply equation (2.46) by $P_{l'}(u_z)$, then we have

$$\begin{aligned} P_{l'}(u_z)P_l(u_z)\partial_s q_l(z,s) + l_c P_1(u_z)P_l(u_z)P_{l'}(u_z)\partial_z q_l(z,s) = \\ -\frac{l_c}{2l_p} l(l+1)P_l(u_z)P_{l'}(u_z)q_l(z,s) - w(z)q_l(z,s)P_l(u_z)P_{l'}(u_z) \end{aligned} \tag{2.47}$$

By integrating over u_z, we then have

$$\begin{aligned} \frac{2}{2l+1}\delta_{ll'}\partial_s q_l(z,s) + 2l_c\Gamma^2_{1,l,l'}\partial_z q_l(z,s) = \\ -\frac{l_c}{2l_p} l(l+1)\frac{2}{2l+1}\delta_{ll'}q_l(z,s) - \frac{2}{2l+1}w(z)\delta_{ll'}q_l(z,s) \end{aligned} \tag{2.48}$$

After that, we can multiply by $\frac{2l+1}{2}$, which gives

$$\begin{aligned} \delta_{ll'}\partial_s q_l(z,s) + (2l+1)l_c\Gamma^2_{1,l,l'}\partial_z q_l(z,s) = \\ -\frac{l_c}{2l_p} l(l+1)\delta_{ll'}q_l(z,s) - w(z)\delta_{ll'}q_l(z,s) \end{aligned} \tag{2.49}$$

In order to make the equation simpler, we define the constant $c \equiv \frac{l_c}{2l_p}$ and $\psi_{1,l,l'} = (2l+1)\Gamma^2_{1,l,l'}$. Thus, we have

$$\begin{aligned} \delta_{ll'}\partial_s q_l(z,s) + l_c\psi_{1,l,l'}\partial_z q_l(z,s) = \\ -cl(l+1)\delta_{ll'}q_l(z,s) - w(z)\delta_{ll'}q_l(z,s) \end{aligned} \tag{2.50}$$

We can write equation (2.50) in the matrix notation,

$$\partial_s q + l_c\psi_1\partial_z q = -cLq - wq \tag{2.51}$$

where L is a diagonal matrix with elements $l(l+1)$. Now, we differentiate equation (2.51) in respect to z. Note that both the partial partition function and the field depend on z, thus we have

$$\partial_s\partial_z q + l_c\psi_1\partial_z^2 q = -cL\partial_z q - w\partial_z q - q\partial_z w \tag{2.52}$$

Similarly, we differentiate equation (2.51) in respect to s. Only the partition function depends on s, and so we have

$$\partial_s^2 q + l_c\psi_1\partial_s\partial_z q = -cL\partial_s q - w\partial_s q \tag{2.53}$$

By combining these two equations, calculating (2.53) $- l_c\psi_1$(2.52), and simplifying, we will be able to omit the $\partial_s\partial_z$ term. By doing so we have

$$\partial_s^2 q = l_c^2\psi_1^2\partial_z^2 q + l_c\psi_1[cL + wI]\partial_z q - [cL + wI]\partial_s q + l_c\psi_1 q\partial_z w \tag{2.54}$$

By adding $\frac{\Delta s}{2}$(2.54) to the right hand side of equation (2.51) we get

$$\begin{aligned}\partial_s q + \frac{\Delta s}{2}\partial_s^2 q = \frac{\Delta s}{2}l_c^2\psi_1^2\partial_z^2 q + l_c\psi_1[\frac{\Delta s}{2}cL + \frac{\Delta s}{2}wI - I]\partial_z q \\ -\frac{\Delta s}{2}[cL + wI]\partial_s q + [\frac{\Delta s}{2}l_c\psi_1\partial_z w - cL - wI]q\end{aligned} \tag{2.55}$$

both $\partial_s q + \frac{\Delta s}{2}\partial_s^2 q$ and $\partial_s q$ can be substituted by D_s, but $\partial_s q + \frac{\Delta s}{2}\partial_s^2 q$ is a better approximation for it. By substituting all the partial derivatives, we have

$$\begin{aligned}D_s q = \frac{\Delta s}{2}l_c^2\psi_1^2 D_{zz} q + l_c\psi_1[\frac{\Delta s}{2}cL + \frac{\Delta s}{2}wI - I]D_z q \\ -\frac{\Delta s}{2}[cL + wI]D_s q + [\frac{\Delta s}{2}l_c\psi_1\partial_z w - cL - wI]q\end{aligned} \tag{2.56}$$

by moving all the terms, which include D_s to the left hand side of the equation, we can rewrite equation (2.56) as

$$\begin{aligned}[I + \frac{\Delta s}{2}cL + \frac{\Delta s}{2}wI]D_s q = \frac{\Delta s}{2}l_c^2\psi_1^2 D_{zz} q + l_c\psi_1[\frac{\Delta s}{2}cL + \\ \frac{\Delta s}{2}wI - I]D_z q + [\frac{\Delta s}{2}l_c\psi_1\partial_z w - cL - wI]q\end{aligned} \tag{2.57}$$

Now, we can define new variables in order to make the equation simpler.

$$A \equiv \frac{1}{\Delta s}I + \frac{1}{2}cL + \frac{1}{2}wI \tag{2.58a}$$

$$B \equiv \frac{\Delta s}{\Delta z^2}\frac{1}{2}l_c^2\psi_1^2 \tag{2.58b}$$

$$C \equiv \frac{\Delta s}{2\Delta z}l_c\psi_1[\frac{1}{2}cL + \frac{1}{2}wI - \frac{1}{\Delta s}I] \tag{2.58c}$$

$$E \equiv \frac{\Delta s}{2}l_c\psi_1\partial_z w - cL - wI \tag{2.58d}$$

Now, with these new variables, the equation can be written as

$$\Delta s A D_s q = (\Delta z)^2 B D_{zz} q + 2\Delta z C D_z q + Eq \tag{2.59}$$

Here again, we assume $i = s$, $i+1 = s+\Delta s$, $j = z$ and $j+1 = z+\Delta z$, so we can rewrite the derivatives in this way,

$$D_s q = \frac{1}{\Delta s}(q^{i+1,j} - q^{i,j}) \tag{2.60a}$$

$$D_z q = \frac{1}{2\Delta z}(q^{i,j+1} - q^{i,j-1}) \tag{2.60b}$$

$$D_{zz} q = \frac{1}{\Delta z^2}(q^{i,j+1} - 2q^{i,j} + q^{i,j-1}) \tag{2.60c}$$

By substituting (2.60) in equation (2.59), we obtain

$$A(q^{i+1,j} - q^{i,j}) = B(q^{i,j+1} - 2q^{i,j} + q^{i,j-1}) + C(q^{i,j+1} - q^{i,j-1}) + Eq^{i,j} \tag{2.61}$$

We now rearrange this into a recursion relation for $q^{i+1,j}$ involving $q^{i,j}$ for all j. This gives

$$q^{i+1,j} = A^{-1}[B - C]q^{i,j-1} + A^{-1}[A + E - 2B]q^{i,j} + A^{-1}[C + B]q^{i,j+1} \tag{2.62}$$

After calculating partition function, the canonical ensemble is used in order to calculate concentration. For single partition function, Q, we have

$$Q = \int_{-1}^{1} du_z \int dz q(z, u_z, s) q(z, -u_z, 1 - s) \tag{2.63}$$

If we write partition functions by applying equation (2.38) then we have

$$Q_l = \int_{-1}^{1} du_z P_l(u_z) P_{l'}(-u_z) \int dz q_l(z, s) q_{l'}(z, 1 - s) \tag{2.64}$$

One can substitute $P_{l'}(-u_z)$ with $(-1)^{l'} P_{l'}(u_z)$, and then by the use of equation (2.34) for $l = l'$, we have

$$Q_l = (-1)^l \frac{2}{2l+1} \int dz q_l(z, s) q_{l'}(z, 1 - s) \tag{2.65}$$

Then, for concentration, we have

$$\phi(z) = \frac{D}{Q}\int_{-1}^{1} du_z \int_{0}^{1} dsq(z, u_z, s)q(z, -u_z, 1-s) \tag{2.66}$$

which can be written as

$$\phi_l(z) = \frac{D}{Q}\int_{-1}^{1} P_l(u_z)P_{l'}(-u_z)du_z \int_{0}^{1} dsq_l(z, s)q_{l'}(z, 1-s) \tag{2.67}$$

Similarly, this reduces to

$$\phi_l(z) = (-1)^l \frac{2}{2l+1}\frac{D}{Q}\int_{0}^{1} dsq_l(z, s)q_{l'}(z, 1-s) \tag{2.68}$$

Thus, we have

$$\phi_i(z) = \frac{n_i}{n}\sum_l (-1)^l \frac{2}{2l+1}\frac{D}{Q}\int_{0}^{1} dsq_l(z, s)q_{l'}(z, 1-s) \tag{2.69}$$

2.4 Anderson mixing

For the field calculation, we begin with an initial guess for $w(z)$. From that, we can produce an improved field which is closer to the actual field. By continuing this iteration, the error becomes smaller until it is within our chosen tolerance. Then, the calculation will be finished.

There are several methods to generate a new field in a way that will be closer to the actual one, but in this work, simple mixing and Anderson mixing were used. Simple mixing works slowly, but it is a stable technique. On the other hand, Anderson mixing works faster, but it is not as stable. As a result, when the error is large, a simple mixing method is used. When the error becomes sufficiently small, we switch to Anderson mixing. There are several related works that used this method [91, 92, 93].

The first step is to determine the deviation from the reference concentration,

$$d_j^{(k)} = \phi_{1,j} + \phi_{2,j} - \phi_{\mathrm{ref,j}} \tag{2.70}$$

where d stands for deviation and k is the iteration number. Our final goal here is to make this deviation close enough to zero. In the simple mixing method, the new field is obtained from

$$w_j^{(k+1)} = w_j^{(k)} + \lambda d_j^{(k)} \tag{2.71}$$

where λ is a mixing parameter.

This method is so time consuming, which is why Anderson mixing method is applied [94]. The error can be defined as

$$error \equiv \left[\frac{1}{M} \sum_j (d_j^{(k)})^2 \right]^{1/2} \tag{2.72}$$

We define a symmetric matrix

$$U_{mn} = \sum_j (d_j^{(k)} - d_j^{(k-m)})(d_j^{(k)} - d_j^{(k-n)}), \tag{2.73}$$

where $m, n = 1, ..., n_r$ and n_r is the number of preceding iterations.

$$V_m = \sum_j (d_j^{(k)} - d_j^{(k-m)}) d_j^{(k)} \tag{2.74}$$

Now, for all histories, we calculate the coefficient.

$$C_n = \sum_m (U^{-1})_{nm} V_m \tag{2.75}$$

where n is the number of histories. At first, previous histories should be combined.

$$W_j^{(k)} = w_j^{(k)} + \sum_{n=1}^{n_r} C_n (w_j^{(k-n)} - w_j^{(k)}) \tag{2.76}$$

$$D_j^{(k)} = d_j^{(k)} + \sum_{n=1}^{n_r} C_n (d_j^{(k-n)} - d_j^{(k)}) \tag{2.77}$$

The new field is then given by

$$w_j^{(k+1)} = W_j^{(k)} + \lambda D_j^{(k)} \tag{2.78}$$

As λ gets larger, iterations converge faster, but they are less stable and that convergence requires an accurate initial guess.

Chapter 3

Results

3.1 SCFT of the Gaussian chain model

This section describes Gaussian chain results in detail. In this model, the only parameter, which could be changed, is the end-to-end distance of both polymer components, $R_{0,1}$, and $R_{0,2}$. The final objective in the following pages is to illustrate the concentration and the excess concentration profiles. We will discover that the profiles can be scaled so as to collapse onto a universal curve, when $R_{0,1}, R_{0,2} \gg \xi$ and $R_{0,1} \approx R_{0,2}$.

3.1.1 Different end-to-end lengths

As was mentioned in the earlier chapters, in a binary polymer blend, different properties of the two components may lead to segregation of one component to the surface. However, in this work, the focus is on segregation due to entropic effects. This section, considers binary polymer blends where the two components have different end-to-end distances. The first question is which of the two components segregates to the surface? In order to answer this question, we take the example of a binary blend with $R_{0,1} = 10\xi$ and $R_{0,2} = 20\xi$. Figure 3.1 shows the concentration profile for this case.

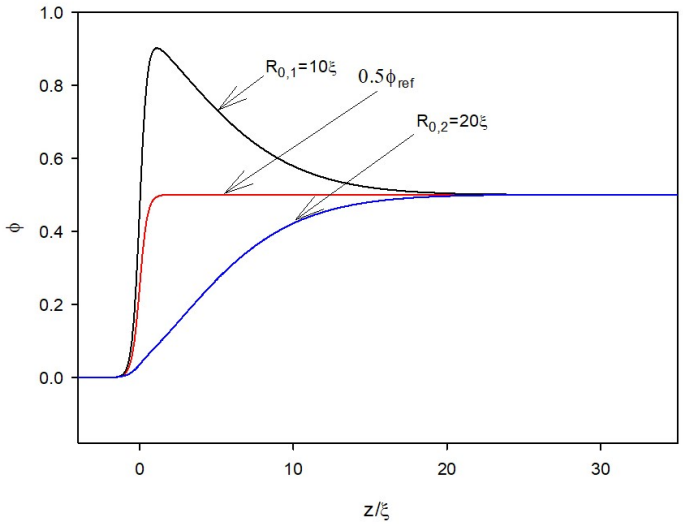

Figure 3.1: Concentration profile. The red curve shows the concentration of each polymer component if there is no segregation in the blend. The black curve and the blue curve are for polymers with an end-to-end distance equal to 10ξ and 20ξ, respectively.

As clearly evident in figure 3.1, the polymer component with a smaller end-to-end distance segregates to the surface. One important quantity in this regard is the excess concentration, which is the difference between the black and the red curves in figure 3.1 (which is also equal to the difference between the red and blue curves) and could be calculated as follows,

$$\phi_{\text{ex}}(z) = \phi(z) - 0.5\phi_{\text{ref}}(z) \tag{3.1}$$

The excess concentration profile associated with figure 3.1 is shown in the figure 3.2.

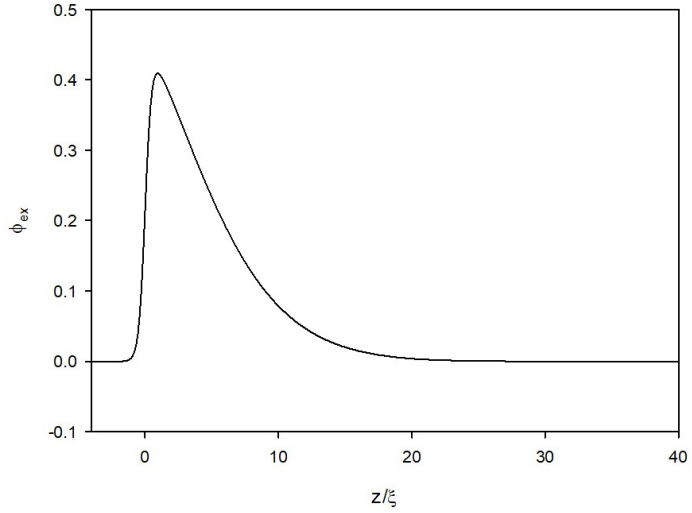

Figure 3.2: Excess concentration profile ($R_{0,1} = 10\xi$ and $R_{0,2} = 20\xi$)

The area under the curve shown in figure 3.2 is referred to as the integrated excess, which is calculated as follows,

$$\Theta_{\text{ex}} = \rho_0 \int \phi_{\text{ex}}(z) dz \tag{3.2}$$

where ρ_0 is the bulk segment density. In regard to figure 3.2, there are several points that should be emphasized. One of these points is the peak height which we denote by Φ_{max}, and the other is the point where we reach bulk concentration, which we denote by z_{bulk}. Naturally, we approach the bulk properties gradually and not at one exact point. Therefore, we consider this point as a point where the excess concentration drops to 10^{-4}.

Other than determining which component segregates to the surface, we are interested in investigating the trend as well. In the next step, $R_{0,1}$ is kept the same but $R_{0,2}$ is different in each case. As $R_{0,2}$ increases, Φ_{max} and z_{bulk} increase implying that the segregation becomes more pronounced.

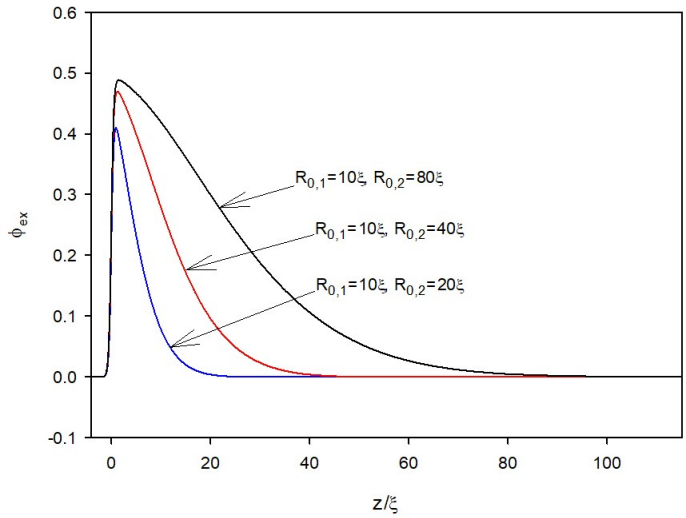

Figure 3.3: Excess concentration ($R_{0,1} = 10\xi$ and $R_{0,2} = 2R_{0,1}, 4R_{0,1}, 8R_{0,1}$ for blue, red and black curves, respectively.)

Figure 3.3 shows three cases; in all the cases $R_{0,1} = 10\xi$ and $R_{0,2}$ increases from 20ξ to 40ξ to 80ξ. Increasing the end-to-end distance of the second polymer increases the peak height and the integrated excess. These parameters could help us in comparing the plots quantitatively. The peak height is 0.41, 0.47 and 0.49 and the integrated excess is 2.74, 6.36 and 13.57 for the case with $R_{0,2} = 2R_{0,1}$, $4R_{0,1}$ and $8R_{0,1}$, respectively.

In the previous case, we kept $R_{0,1}$ the same and increased $\frac{R_{0,2}}{R_{0,1}}$. The question which is brought up here is whether the mentioned ratio is the only parameter that controls the shape of the profile. In order to check, we can consider three different cases with the same $\frac{R_{0,2}}{R_{0,1}}$ but different $R_{0,1}$ and $R_{0,2}$.

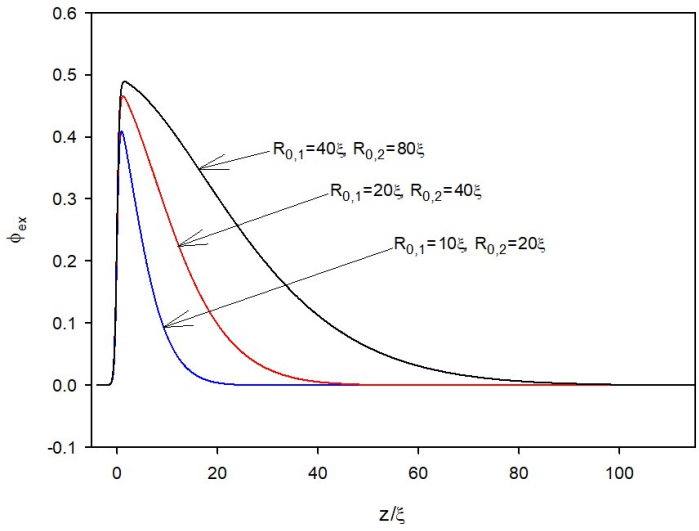

Figure 3.4: Excess concentration profile ($\frac{R_{0,2}}{R_{0,1}} = 2$, $R_{0,1} = 10\xi, 20\xi$, and 40ξ for blue, red and black curves, respectively.)

Figure 3.4 shows three cases with a constant value of $\frac{R_{0,2}}{R_{0,1}}$ but different average end-to-end lengths. The figure illustrates the effect of average end-to-end distance on the profile shape. As the average end-to-end distance increases, the peak height and integrated excess increase as well. The peak height is 0.41, 0.47 and 0.49 and the integrated excess is 2.74, 6.38 and 13.91 for $R_{0,1}$ equal to 10ξ, 20ξ and 40ξ, respectively.

3.1.2 Universal plot

This section will show that the excess concentrations can be collapsed onto a universal curve, under appropriate conditions. The objective here is to predict the peak height and integrated excess for a blend just by knowing the end-to-end distances of two polymer components. This will be possible by the use of the universal plot. In order to reveal the universality, the effect of different parameters need to be studied. As it described at the beginning of this chapter, we have only two parameters which are the end-to-end distances for both polymers. We define our parameters in another way;

$$R_{\text{avg}} = \frac{R_{0,1} + R_{0,2}}{2} \tag{3.3}$$

$$\Delta R = R_{0,2} - R_{0,1} \tag{3.4}$$

where R_{avg} is the average of two end-to-end lengths of the two polymer components and ΔR is their difference. In order to attain the mentioned universal plot, one of these parameters should be kept the same and the effect of another one should be studied. The universal plot may not be extremely precise for all the values of R_{avg} and ΔR, and thus investigating the deviation would be the next objective.

Effect of ΔR

In order to study the effect of ΔR, we keep R_{avg} the same and change ΔR, as shown in figure 3.5.

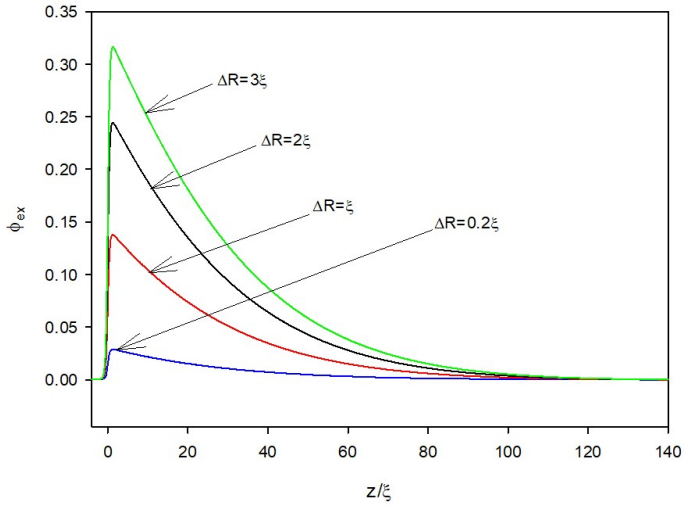

Figure 3.5: Excess concentration profile. ($R_{\text{avg}} = 100\xi$ for all the cases and ΔR=0.2ξ, ξ,2ξ and 3ξ for blue, red, black and green curves, respectively.)

Figure 3.5 shows that by increasing ΔR, Φ_{max} increases but z_{bulk} remains constant for all the cases. We conclude that in the case of different ΔR, only the vertical axis needs to be scaled. The scaling can be done by dividing the peak height by ΔR.

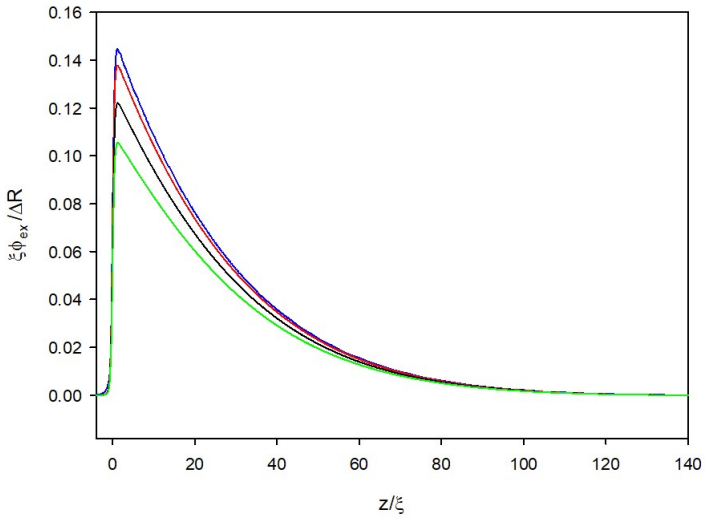

Figure 3.6: Excess concentration profile with scaled vertical axis. ($R_{\text{avg}} = 100\xi$ for all the cases and ΔR=0.2ξ, ξ,2ξ and 3ξ for blue, red, black and green curves, respectively.)

As it is shown in figure 3.6, after scaling, the discrepancy between different curves decreases. Generally, it could be comprehended from this figure that as the ΔR increases the scaled peak height decreases. The blue and red curves, which are associated with $\Delta R = 0.2\xi$ and $\Delta R = \xi$, have similar peak heights after scaling despite the fact that ΔR for one of them is roughly five times that of the other. However, for the case of $\Delta R = 3\xi$, there is significant deviation from other curves, which will be illustrated in the following figures.

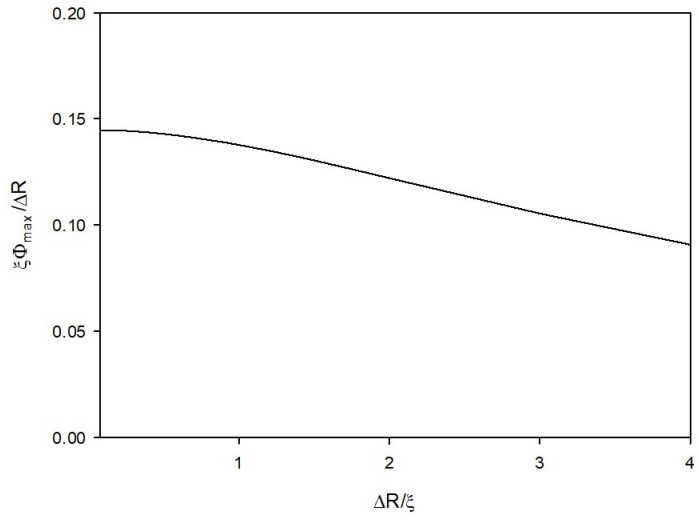

Figure 3.7: Scaled peak height versus $\frac{\Delta R}{\xi}$

Figure 3.7 shows the scaled peak height versus $\frac{\Delta R}{\xi}$. For $\frac{\Delta R}{\xi}$ smaller than 1, the curve is roughly horizontal, but as $\frac{\Delta R}{\xi}$ increases, the scaled peak height decreases, implying that for large values of $\frac{\Delta R}{\xi}$ we would have significant deviation from the universal plot.

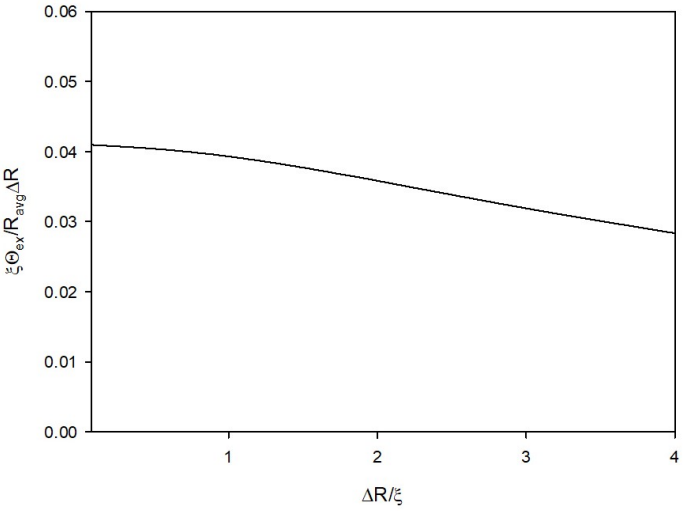

Figure 3.8: Scaled integrated excess versus $\frac{\Delta R}{\xi}$

Figures 3.7 and 3.8 show the scaled peak height and integrated excess versus $\frac{\Delta R}{\xi}$, respectively. As illustrated by these figures, the scaling works in a particular range and as ΔR gets larger the deviation from the universal plot increases.

Effect of R_{avg}

In the following section, the effect of R_{avg} is illustrated.

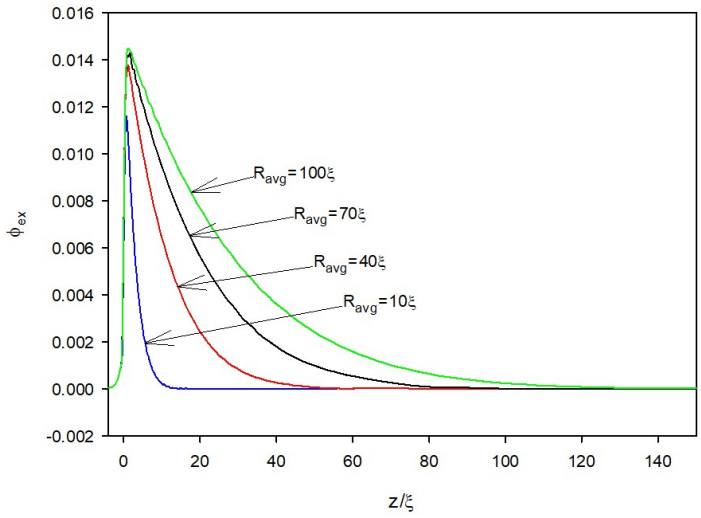

Figure 3.9: Excess concentration profile. (In all the cases, $\Delta R = 0.1\xi$ and $R_{\text{avg}} = 10\xi, 40\xi, 70\xi$,and 100ξ for blue, red , black and green curves, respectively)

Figure 3.9 shows that by increasing R_{avg}, the peak height initially increases but as the average end-to-end distance increases the peak height converges to a universal value. This makes sense since, as it was mentioned previously, the Gaussian chain model works well for long chains with high molecular weights. Hence, the results will be more realistic as the chains become longer. As a result, if R_{avg} is sufficiently large, changing that does not affect the peak height and only changes z_{bulk}. Hence, in this case, the horizontal axis should be scaled. As a result, it is clear that in order to collapse the curves onto a universal plot, the polymers should have large R_{avg} and small ΔR.

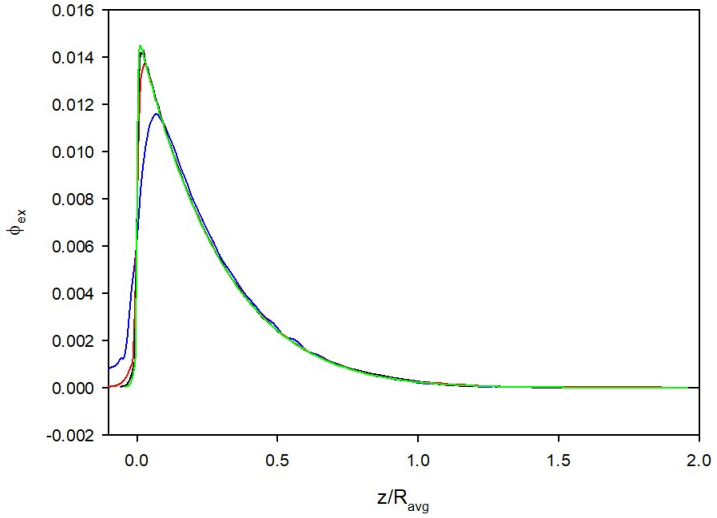

Figure 3.10: Excess concentration profile with scaled horizontal axis. (In all the cases $\Delta R = 0.1\xi$ and $R_{\text{avg}} = 10\xi, 40\xi, 70\xi$,and 100ξ for blue, red , black and green curves, respectively)

As figure 3.10 shows, after scaling, the discrepancy between plots decreases. Only for the case of $R_{\text{avg}} = 10\xi$ is significant deviation from other curves, which is due to the small R_{avg} as discussed previously.

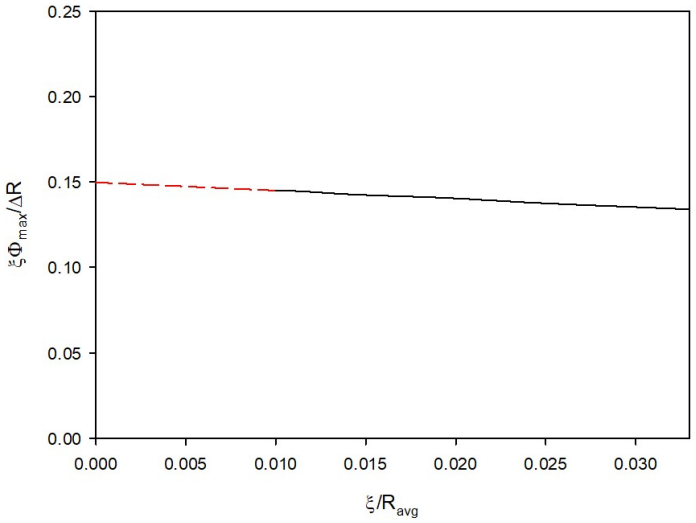

Figure 3.11: Scaled peak height versus $\frac{1}{R_{\text{avg}}}$

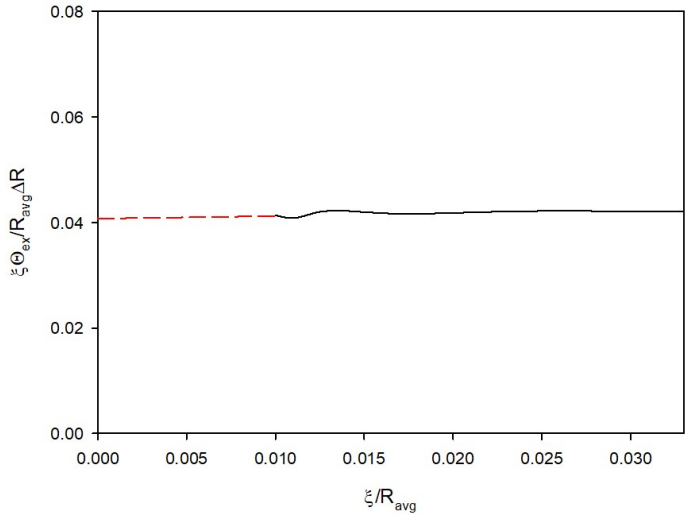

Figure 3.12: Scaled integrated excess versus $\frac{1}{R_{\text{avg}}}$

Figures 3.11 and 3.12 show how the peak height and integrated excess change with respect to $\frac{\xi}{R_{\text{avg}}}$. By considering the polymers with $\frac{R_{\text{avg}}}{\xi}$ more than 50 and extrapolating, the peak height and integrated excess for the universal plot are found to be $0.15\frac{\Delta R}{\xi}$

and $0.041\frac{R_{\text{avg}}\Delta R}{\xi}$, respectively. In the next step, three different cases are considered with different ΔR and R_{avg}.

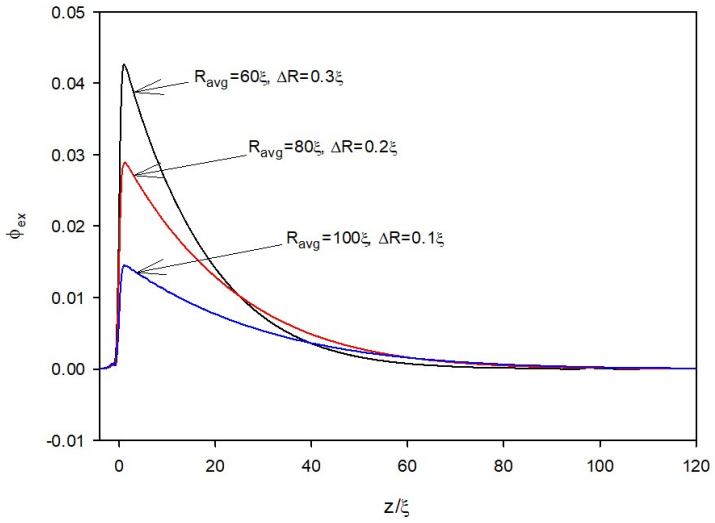

Figure 3.13: Excess concentration profile. $((R_{\text{avg}}, \Delta R)$ is $(100\xi, 0.1\xi)$, $(80\xi, 0.2\xi)$ and $(60\xi, 0.3\xi)$ for the blue, red and black curves, respectively)

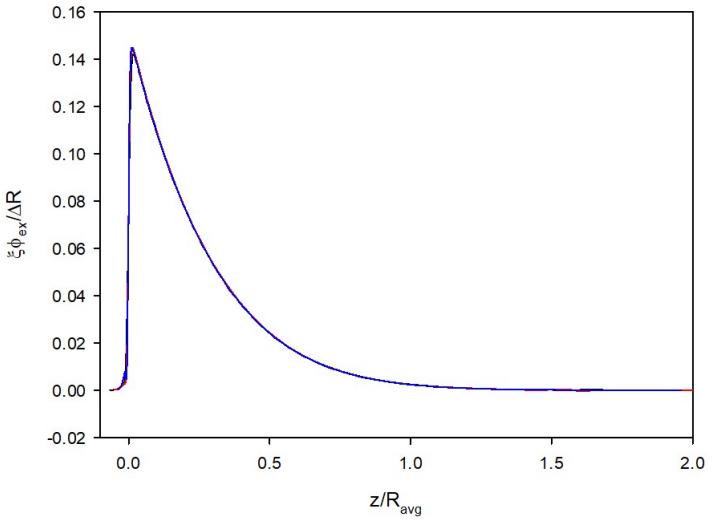

Figure 3.14: Scaled excess concentration profile. $((R_{\text{avg}}, \Delta R)$ is $(100\xi, 0.1\xi)$, $(80\xi, 0.2\xi)$ and $(60\xi, 0.3\xi)$ for the blue, red and black curves, respectively)

As figure 3.13 illustrates, different cases have different $\Phi_{\max}$ and z_{bulk}, but after scaling, the plots collapse as illustrated in figure 3.14. These two figures confirm the effectiveness of the universal plot in the acceptable range.

3.2 SCFT of the worm-like chain model

The remaining part of this chapter deals with the worm-like chain results. In this model, unlike the Gaussian chain model, we have four parameters; contour length and persistence length of each of the two polymer components, which could be either similar or different in different case studies. In order to compare this model with the Gaussian chain model, we need to know how their parameters are related. End-to-end distance can be calculated based on contour and persistence length with the below formula,

$$R_0 = \sqrt{2l_p l_c}\sqrt{(1 - \frac{l_p}{l_c}[1 - \exp(-\frac{l_c}{l_p})])} \tag{3.5}$$

The second square root is a correction factor and as was stated in the previous chapter, for long chains, where $l_c \gg l_p$, this formula can be simplified.

$$R_0 = \sqrt{2l_c l_p} \tag{3.6}$$

In all the cases that we consider here, we have at least 10 persistence lengths along the polymer chain, which means that the simplified formula will be within 5% accuracy.

3.2.1 Same persistence length, different contour lengths

Initially, persistence length is kept the same and the effect of contour length is studied. Figure 3.15 shows the profiles for a binary polymer blend with one polymer shorter than the other. The component with a shorter contour length segregates to the surface. As the contour length decreases, the end-to-end distance decreases as well, and based on the Gaussian chain results the polymer component with a shorter end-to-end distance segregates to the surface. This means that the results for these two models are compatible qualitatively. The results will be compared quantitatively as well at the end of this chapter.

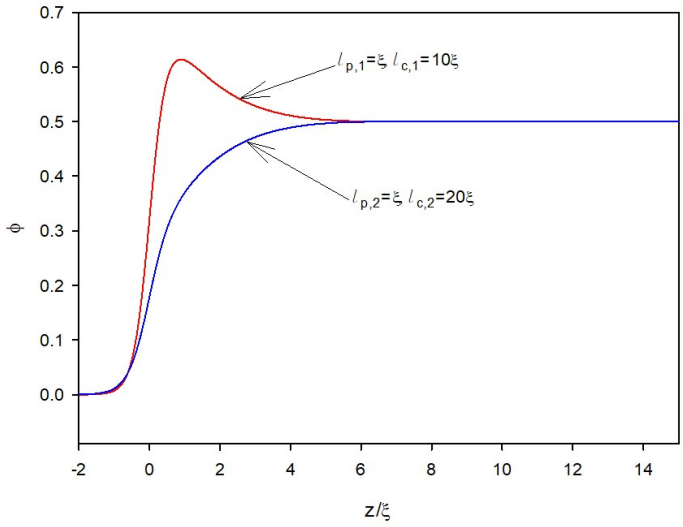

Figure 3.15: Polymer concentration profile. ($l_p = \xi$, $l_{c,1} = 10\xi$ and $l_{c,2} = 20\xi$ for red and blue curves, respectively)

The other interesting perspective is to study the trend by increasing the difference of two contour lengths. It could be done by keeping $l_{c,1}$ the same and increasing $l_{c,2}$.

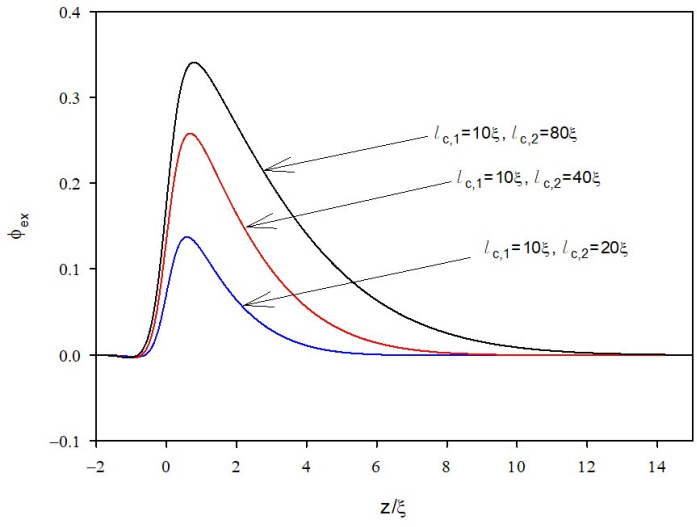

Figure 3.16: Excess concentration profile. ($l_{c,1} = 10\xi$ and $l_{c,2} = 2l_{c,1}$, $4l_{c,1}$, $8l_{c,1}$ for blue, red and black curves, respectively)

Figure 3.16 shows that as the discrepancy between contour lengths of the two polymers increases, Φ_{bulk} and z_{bulk} increase as well. In the next step, the ratio of two contour lengths is kept constant but their average is different in each case. This time, we compare the results with the Gaussian chain model quantitatively.

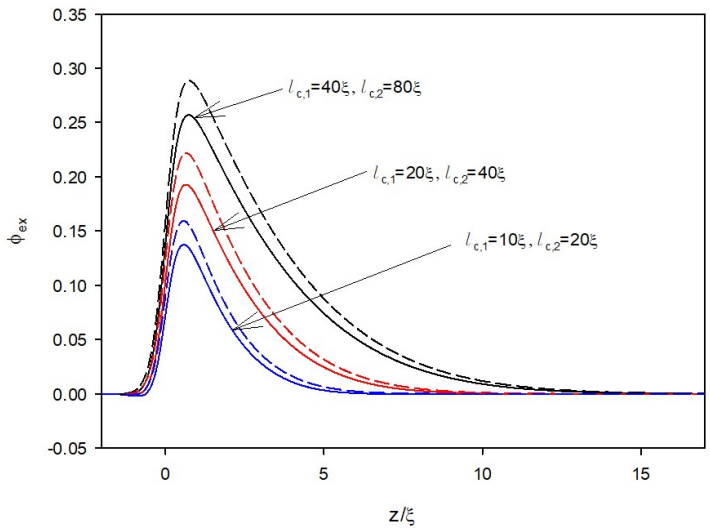

Figure 3.17: Excess concentration profile. The solid curve shows the worm-like chain and the dashed curve shows the Gaussian chain results. Curves with the same color correspond to the same input parameters. (In all the cases $l_p = \xi$ and $\frac{l_{c,2}}{l_{c,1}} = 2$. The contour lengths for the first polymer are 10ξ, 20ξ and 40ξ for the blue, red and black curves, respectively.)

Figure 3.17 shows the trend caused by changing the contour length. In all cases, the ratio of two contour lengths is constant but the average contour length is different. Both models predict that by increasing this value, Φ_{max} and z_{bulk} increase as well. Φ_{max}, predicted by the Gaussian chain model, is larger than the worm-like chain model. As the polymers become longer, the error decreases. Hence, for the black curve, the discrepancy between the two models is least. It is worth mentioning that we have at least 40, 20, and 10 persistence lengths in the black, red, and blue curves, respectively (for the polymer component with a minimum number of persistence lengths).

3.2.2 Same contour length, different persistence lengths

In the following pages, the contour length is kept constant, and the effect of persistence length is studied. As figure 3.18 illustrates, the surface is rich in the polymer component with smaller persistence length (i.e. the more flexible polymer component). Figure 3.18 shows a binary polymer blend where the two contour lengths are both equal to 40ξ. However, they are different in persistence length. As shown in the figure, the surface is rich in the polymer with the smaller persistence length, which is equal to ξ rather than the one with larger persistence length.

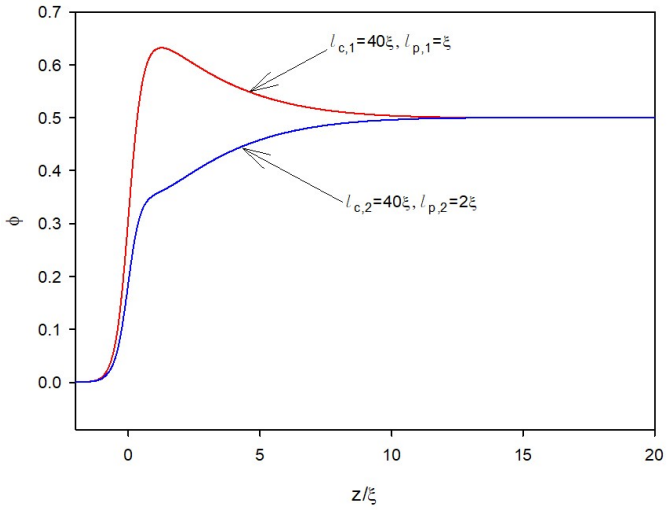

Figure 3.18: Concentration profile ($l_c = 40\xi$ and $l_{p,1} = \xi$, $l_{p,2} = 2\xi$ for red and blue curves, respectively.)

As in the previous section, we now study the trend.

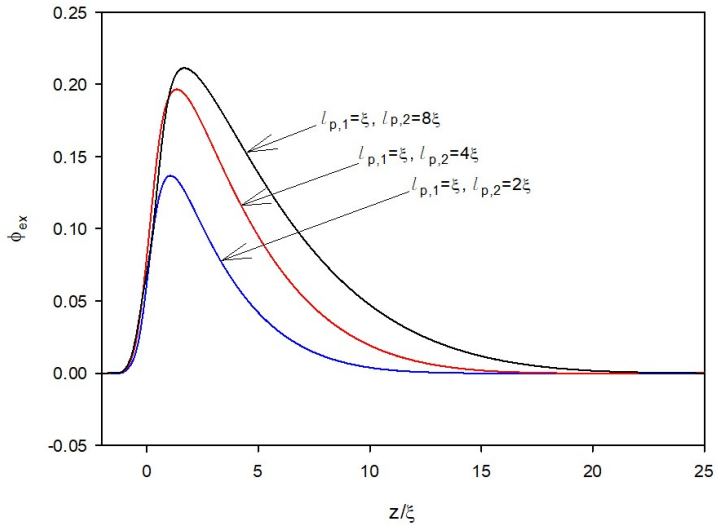

Figure 3.19: Excess concentration profile ($l_c = 40\xi$ and $l_{p,1} = \xi$ for all cases and $l_{p,2} = 2l_{p,1}$, $4l_{p,1}$, $8l_{p,1}$ for blue, red and black curves, respectively.)

Figure 3.19 shows that as we increase the difference between the persistence lengths of two polymer components, $\Phi_{\max}$ and z_{bulk} both increase. Generally, as the polymer becomes stiffer (i.e. persistence length increases), the end-to-end distance increases as well. As a result, the worm-like chain model predicts that the more flexible polymer (i.e. the polymer with shorter end-to-end length) segregates to the surface, which is consistent with the Gaussian chain results.

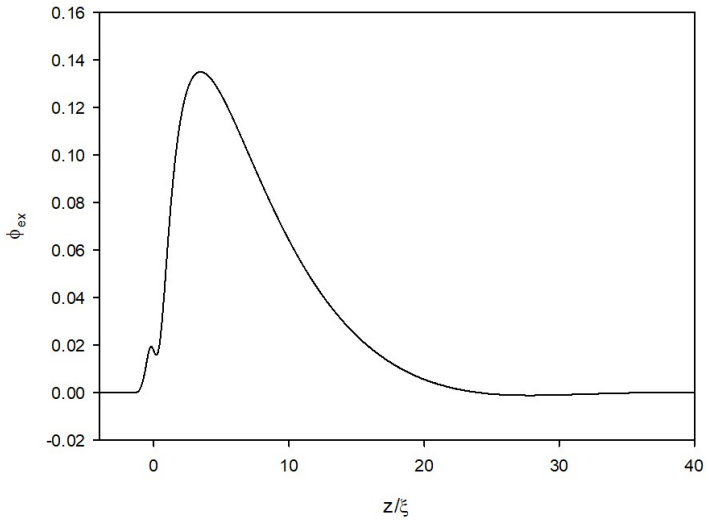

Figure 3.20: Excess concentration profile ($l_c = 40\xi$, $l_{p,1} = 2\xi$ and $l_{p,2} = 16\xi$)

As the polymer components become stiffer, the excess concentration profile develops an unusual local maximum near $z \approx 0$ (figure 3.20). However, by looking at the concentration profile (figure 3.21), it is evident that this profile is reasonable as two concentrations are similar up to $z \leq 0$ and after that, there is a drop in the concentration of the stiffer component.

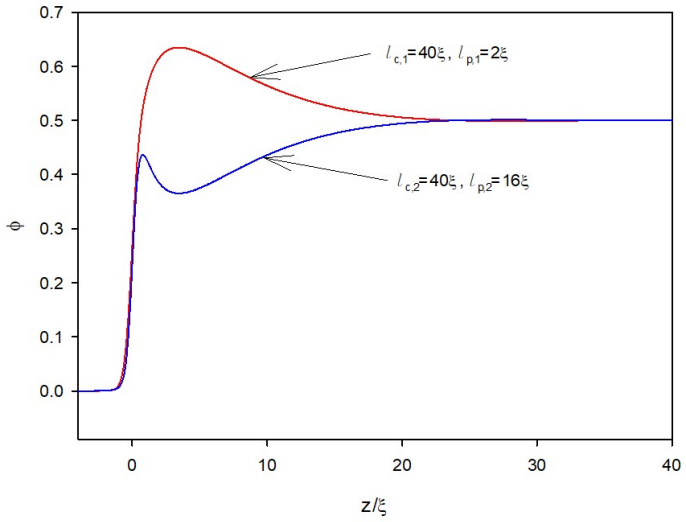

Figure 3.21: Concentration profile ($l_c = 40\xi$, $l_{p,1} = 2\xi$ and $l_{p,2} = 16\xi$ for red and blue curves, respectively.)

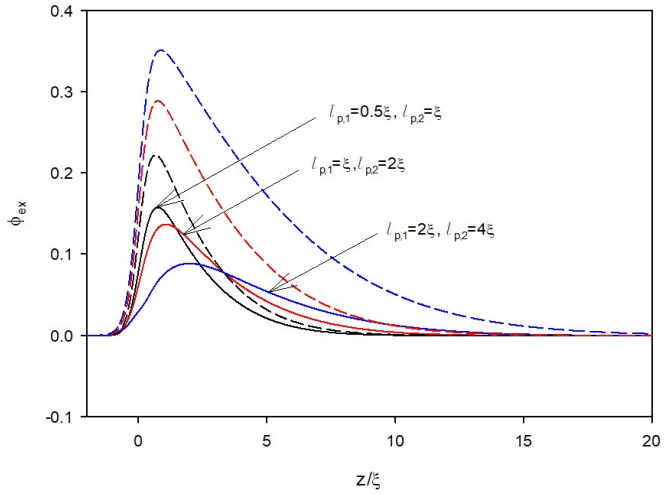

Figure 3.22: Excess concentration profile. The solid curve shows the worm-like chain and the dashed curve shows the Gaussian chain results. Curves with the same color correspond to the same parameters ($l_c = 40\xi$ and $\frac{l_{p,2}}{l_{p,1}} = 2$, $l_{p,1} = 0.5\xi, \xi$,and 2ξ for black, red and blue curves, respectively.)

Figure 3.22 shows that according to the worm-like chain model, if the polymers are more flexible (i.e. shorter end-to-end distance) $\Phi_{\max}$ is larger, which is contrary to what the Gaussian chain model predicts. It is worth mentioning that as the polymers become more flexible, the results of the two models become closer. This trend makes sense since the Gaussian chain model assumes the polymers are completely flexible. Hence, as two components in the worm-like chain get more flexible, the difference between the results decreases.

The minimum number of persistence lengths is 40, 20, and 10 for black, red, and blue curves, respectively (for the polymer component with the least number of persistence lengths). Hence, we could realize that as the number of persistence lengths along the chain increases the results of the two models get closer.

In addition, there is one other difference between these two models. For the Gaussian chain model, as the end-to-end distance increases, $\Phi_{\max}$ and z_{bulk} increase, but that is not true for the worm-like chain model. For this model, in the case where $\Phi_{\max}$ is largest, z_{bulk} is smallest.

One might think that the only important factor here is that the persistence length should be sufficiently small with respect to the contour length. However, another factor that plays a role in this regard is whether the persistence length is smaller than the width of the surface.

Figure 3.23 shows three different cases. In all cases, the contour length is constant and $\frac{l_{p,2}}{l_{p,1}} = 2$. It is worth mentioning as for the previous case, $\Phi_{\max}$ for the Gaussian chain model is larger than that of the worm-like chain model and as the polymers become more flexible, the discrepancy between the two models decreases. Although, unlike figure 3.22, the trend for the worm-like chain model and the Gaussian model is similar, meaning that increasing the stiffness causes $\Phi_{\max}$ and z_{bulk} to increase for both models. One other factor to mention here is that for both models, the curves with larger $\Phi_{\max}$ both have larger z_{bulk}. So, in order for the Gaussian chain model to be accurate, the persistence length should be smaller than any other length (e.g. the contour length and the width of the surface).

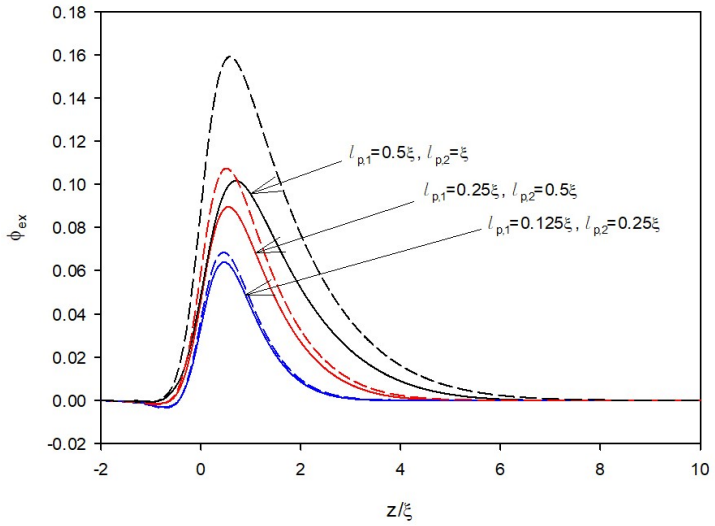

Figure 3.23: Excess concentration profile. The solid curve shows the worm-like chain and the dashed curve shows the Gaussian chain results. Curves with the same color denote the same input parameters ($l_c = 20\xi$ and $\frac{l_{p,2}}{l_{p,1}} = 2$ for all the cases and $l_{p,1} = 0.125\xi$, 0.25ξ and 0.5ξ for blue, red and black curves, respectively.)

3.2.3 Same end-to-end length

In the following chapter, the product of the contour and persistence lengths is kept constant for both polymer components, but their individual values are different in each case. Figure 3.24 illustrates that the shorter and stiffer polymer segregates to the surface and figure 3.25 shows that as the second polymer becomes longer and more flexible the excess concentration increases. The green curve shows the case that the second polymer is totally flexible (i.e. Gaussian chain). It is evident that as the polymer gets longer with a larger number of persistence lengths along the chain, the worm-like results approach the Gaussian chain limit.

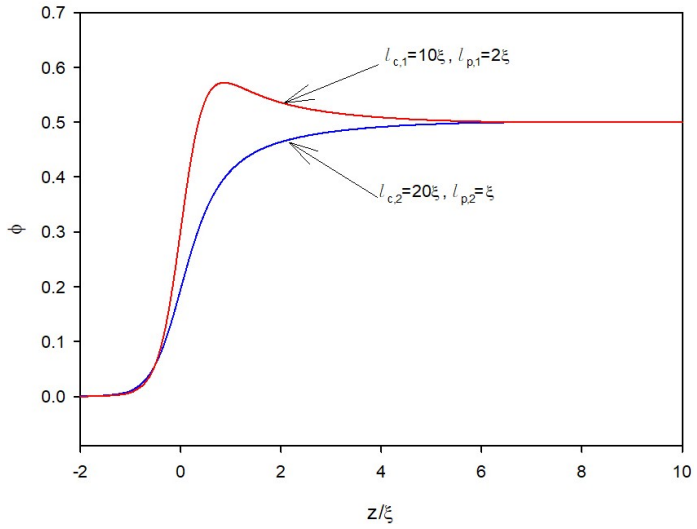

Figure 3.24: Concentration profile ($l_{c,1} = 10\xi$, $l_{p,1} = 2\xi$ and $l_{c,2} = 20\xi$, $l_{p,2} = \xi$ for red and blue curves, respectively.)

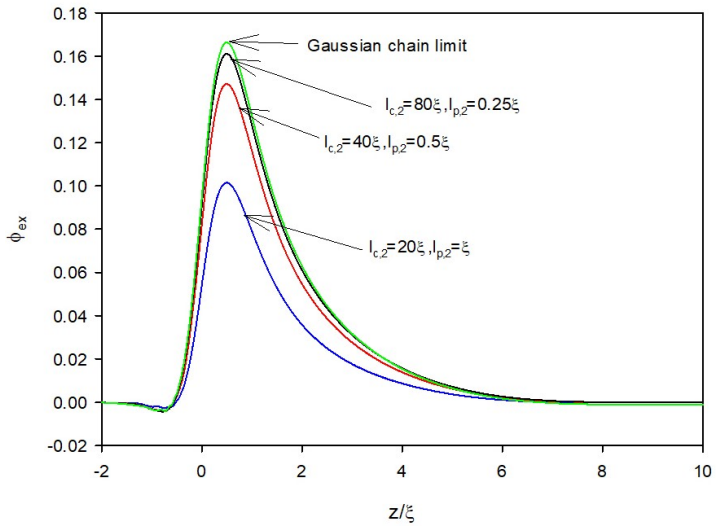

Figure 3.25: Excess concentration profile ($(l_{c,1}, l_{p,1}) = (10\xi, 2\xi)$ and $(l_{c,2}, l_{p,2}) = (20\xi, \xi)$,$(40\xi, 0.5\xi)$ and $(80\xi, 0.25\xi)$ for blue, red and black curves, respectively. The green curve shows the Gaussian chain limit.)

Chapter 4

Conclusion

4.1 Overview

In this thesis, the entropic surface segregation of a binary polymer blend is studied. The blends involve two polymers with the same molecular volume, but different contour lengths, stiffnesses, and thicknesses. The Gaussian chain model [72, 95] and the worm-like chain model [74, 75, 96] are used to represent the polymer chains and study their segregation in each case. SCFT is applied to each model in order to simplify our calculations whereby an external field replaces all the inter-chain interactions acting on a particular polymer.

A general discussion about SCFT is given in Chapter 2. Following that, the external field is determined by enforcing the sigmoidal profile for the concentration and applying Anderson mixing method.

First, the Gaussian chain model is elaborated. In this model, the polymer chain is considered to be thoroughly flexible and the end-to-end distance is our only parameter. A recursion relation for partial partition functions is derived to solve diffusion equation, using the Crank-Nicolson method. Next, the single-chain partition function and concentration of each polymer are calculated and excess concentration and integrated excess are evaluated.

After that, we move on to the worm-like chain model, which includes an energy penalty for bending. In this model, we have two parameters; the contour length and the persistence length. The relationship between these two parameters and the end-to-end distance is given by $R_0 \approx \sqrt{2 l_c l_p}$, and thus increasing the chain length or its stiffness increases the end-to-end distance of the polymer. Finally, the diffusion equation is solved by expanding the partial partition function in terms of Legendre polynomials, and the same steps as for the Gaussian chain model are applied to determine the concentration.

In Chapter 3, initially, the Gaussian chain model results are presented. The only parameters for this model are the end-to-end distance of each polymer. Thus, we go through the case of two components with different end-to-end distances. The results show that the polymer with the smaller end-to-end distance segregates to the surface. Also, if we consider the excess concentration profile, as the discrepancy between two polymer segment lengths increases, $\Phi_{\max}$ and z_{bulk} become larger.

In the next step, the universal plot is developed. For doing so, we define our two parameters as the difference between two end-to-end distances, ΔR, and their average, R_{avg}. First, R_{avg} is kept constant and the effect of ΔR is studied. By increasing ΔR, $\Phi_{\max}$ increases but z_{bulk} remains the same, so only the vertical axis needs to be scaled in this case.

Then, the effect of changing R_{avg} is studied with ΔR held constant. If R_{avg} is sufficiently large, by increasing that only z_{bulk} changes and $\Phi_{\max}$ remains approximately constant. So this time, only the horizontal axis needs to be scaled. After doing so, the universal plot is attained. However, it should be noted that if R_{avg} is too small or ΔR is too large, we will have significant deviations from the universal plot.

Finally, the worm-like chain results are presented. As here we have two parameters per molecule, their effect is studied individually. In the first case, the surface segregation of a polymer blend with different contour lengths is illustrated. In this case, the polymer chain with the shorter contour length segregates to the surface and as the discrepancy between contour lengths increases, $\Phi_{\max}$ and z_{bulk} increase as well. If we keep the ratio of contour lengths the same, while increasing the average contour length, $\Phi_{\max}$ and z_{bulk} increase as was the case for the Gaussian chain model. When the two models are compared, in all the cases the Gaussian chain model shows greater segregation, but the trend agrees qualitatively.

In the next step, we keep the contour length constant and change the persistence length. Increasing persistence length makes the polymer stiffer. In this case, the more flexible polymer segregates to the surface. However, studying the persistence length trend is not as straight forward as the contour length, and it depends on $\frac{l_p}{\xi}$.

If we keep the ratio of the two persistence lengths constant and increase the average persistence length, the trend for the worm-like chain depends on whether $\frac{l_p}{\xi}$ is smaller or larger than one.

If smaller, the trend for the worm-like chain model is same as the Gaussian chain model qualitatively. However, the Gaussian chain still shows larger segregation. Otherwise, the trend for the worm-like chain model is opposite to the Gaussian chain model trend, meaning that for the Gaussian chain model as we increase the average persistence length, $\Phi_{\max}$ and

z_{bulk} of the excess concentration profile increase, while in the worm-like chain model, by increasing the average persistence length, Φ_{max} decreases, but z_{bulk} increases.

We conclude that for the Gaussian chain model to be accurate, the persistence length should be smaller than any other lengths in our system such as the width of the surface or the contour lengths.

The final set of blends considers the case that the end-to-end distance is constant, but the persistence length and the contour length are different, meaning that their product is kept constant. Here, the Gaussian chain model would not predict any segregation, since two segment lengths are equal, but that is not the case for the worm-like chain model. Even if we have the same segment length, we still have segregation due to the difference in the contour and persistence lengths. It is worth mentioning, that in each case, the shorter and stiffer polymer segregates to the surface. Also, as the number of persistence lengths in the longer polymer increases, the results approach the case that the longer polymer is a Gaussian chain.

As was mentioned in detail, the Gaussian chain model has some limitations in the surface segregation prediction due to its initial assumption (i.e. completely flexible chain). Although, the worm-like chain model provides more accurate results, it is far more complicated. Generally, for long flexible polymer chains, it is best to use the Gaussian chain model, but as the polymer chains become stiffer, the worm-like chain model should be used for representing them.

4.2 Areas for improvement

In this work, considerable effort was made to perform a comprehensive study. However, there is always several aspects to enhance a research in one area and make it more general. In the following pages, several aspect of the work, which would benefit from more detailed consideration, are discussed.

4.2.1 Stiffness

Polymer stiffness could vary within a large range. Polymers can be very flexible or virtually rigid [75, 97]; for example, polyethylene or polystyrene, which are synthetic polymers, the persistence length is on the order of $1nm$, while, the value for biopolymers such as filamentous(F-actin), double-stranded(ds) DNA and microtubules is approximately $50nm$ [98].

Stiffness could be quantified [99, 100]. In this work $\frac{l_c}{l_p}$ was used as initial indicator for stiffness. If the mentioned parameter was large enough, it meant that the polymer is flexible and the Gaussian chain model would be accurate. Otherwise, there was a significant deviation between the worm-like chain and Gaussian chain predictions.

As mentioned before, in the worm-like chain model, stiffness is taken into the account. Hence, the worm-like chain model is more precise in predicting segregation for stiff polymers. At the very end of the result section, it was shown, that other than the mentioned ratio, $\frac{l_p}{\xi}$ should be sufficiently small for the Gaussian chain model to work well. In other words, the persistence length should be small in comparison with all other lengths in the system.

Generally, in regards to flexible polymers, it would be realistic to use the Gaussian chain model to represent the polymer chain, but as the polymer becomes stiffer, this model loses its accuracy. The reason that we use both of these models in this work is to do comprehensive research and compare two models. Furthermore, the comparison allows us to quantify the Gaussian chain model accuracy as the polymer chain becomes stiffer.

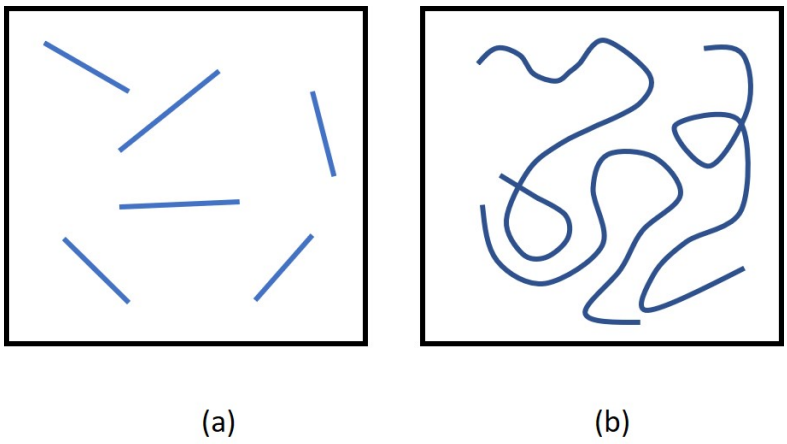

Figure 4.1: (a) Rigid rod (b) Gaussian chain

On the other hand, the polymer stiffness plays a critical role in many applications [101]. As an example, for new sensors, DNA oligonucleotides should be adsorbed on graphene and graphene oxide, and the stiffness of polymers plays a critical role in this adsorption since their bending rigidity is important in this regard [98].

In this work, both the Gaussian chain and worm-like chain models were used to provide a comprehensive perspective in this regard. However, there is still an area for improvement.

In the worm-like chain model section, for defining the partial partition function, it was assumed that it is dependent on the distance from the surface, tangent vector, and backbone parameter.

This assumption could be altered in a way to make the case more comprehensive. By taking azimuthal angle into account, we would be able to consider the effect of the direction that polymers are aligned in as well. By doing so spherical harmonics should be used instead of Legendre polynomials.

4.2.2 Polydispersity

In the case of polymer blends, molecular weight distribution plays a critical role in the blend's properties [102]. Figure 4.2 shows the molecular weight distribution of polymer chains in the blend.

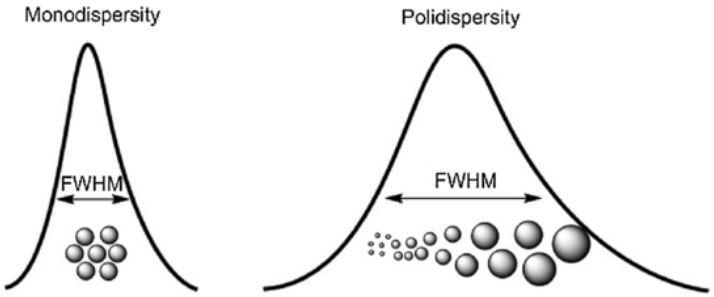

Figure 4.2: Molecular weight distribution [2]

Different molecular weight averages are defined in this field such as number average molecular weight ($\bar{M}_n$), weight average molecular weight ($\bar{M}_w$), viscosity average molecular weight ($\bar{M}_v$) and z-average molecular weight ($\bar{M}_z$). $\bar{M}_n$ highlights the smaller molecules and $\bar{M}_w$ and $\bar{M}_z$ highlight the larger ones. The following formulas are applied to quantify the mentioned values [103, 104].

$$\bar{M}_n = \frac{\sum_i N_i M_i}{\sum_i N_i} \tag{4.1}$$

where N_i denotes the number of molecules with molecular weight equal to M_i. The numerator shows the sample molecular weight and the denominator shows the total number

of polymer molecules [105]. Plastic tensile strength is dependent on $\bar{M}_n$, since smaller molecules have a larger effect on its value, and these molecules do not increase the strength [106].

$$\bar{M}_w = \frac{\sum_i c_i M_i}{\sum_i c_i} \tag{4.2}$$

where c_i is the weight of N_i molecules. Definition of $\bar{M}_v$ is slightly more complicated but its value is smaller than $\bar{M}_w$. Melt viscosity is dependent on $\bar{M}_w$ (in most cases to the power of 3.4), since longer chains are more critical in determining $\bar{M}_v$ [106].

Similarly, $\bar{M}_z$, which is used for polymer rheology and polymer processing, is defined as

$$\bar{M}_z = \frac{\sum_i N_i M_i^3}{\sum_i N_i M_i^2} \tag{4.3}$$

If all the molecular averages are equal, the blend would be a monodisperse blend.

$$\bar{M}_n = \bar{M}_w = \bar{M}_z \tag{4.4}$$

On the other hand, we have polydisperse blends consisting of different molecular weights. In this case, the average molecular weights are not equal anymore.

$$\bar{M}_n < \bar{M}_v < \bar{M}_w < \bar{M}_z \tag{4.5}$$

Needless to say, all the polydisperse polymer blends are not the same, and thus one should define a parameter to quantify the polydispersity. The polydispersity index (PDI) is the measure of molecular weight profile broadness, which is defined as

$$PDI = \frac{\bar{M}_w}{\bar{M}_n} \geq 1 \tag{4.6}$$

For monodisperse blends, PDI is equal to one. Figure 4.3 is a visual representation of the monodisperse and polydisperse concept.

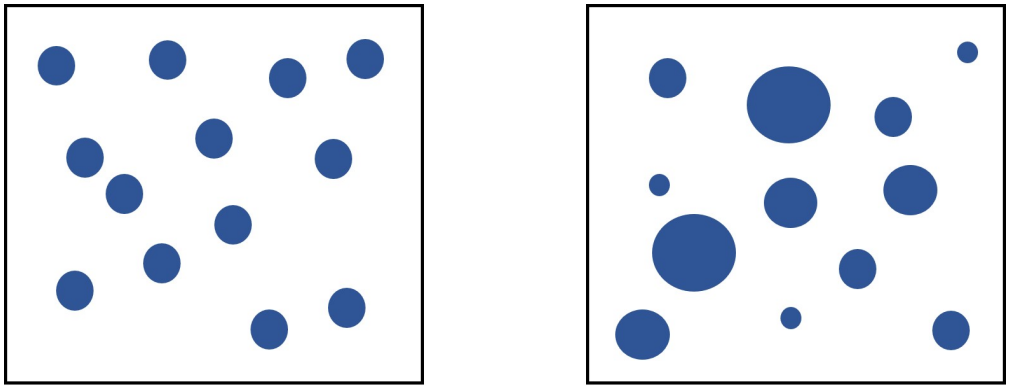

Figure 4.3: If polymer chains could be represented by circles, (a) shows a monodisperse blend and (b) shows a polydisperse blend.

In this research, we study the behavior of binary polymer blend where our two components are monodisperse. Although, a complete monodisperse polymer blend is rare. The polydispersity index for most polymers is between 2 to 15, so it would be nice to consider this fact in future works.

In addition to average molecular weight, molecular weight distribution plays an essential role in polymer's behavior [107]. Polymer blends could have the same polydispersity index but different molecular weight distributions, which leads to different properties.

4.2.3 Packing effect

Based on the results of this work, if two components have the same contour length but different persistence lengths, the one which has a smaller persistence length (i.e. the one which is more flexible) segregates to the surface. However, if the polymers have the same end-to-end distance but different persistence lengths, the one with a larger persistence length (i.e. the one which is stiffer) segregates to the surface.

These results were attained using the worm-like chain model since in this model we have the power to control the persistence length and contour length individually. However, for the Gaussian chain model, the only parameter is the end-to-end distance which would increase either by increasing the contour length or the persistence length, meaning that if we have either long or stiff polymer chains, in both cases the end-to-end distance would be

large. In other words, if the end-to-end distance is a considerable value, there is no way to know if the contour length is responsible or the persistence length.

Yethiraj used Monte Carlo simulations and integral equation theory to predict the surface segregation of a binary polymer blend, in which one component is stiffer than the other [58]. In their work, an athermal system was used to exclude enthalpic effects thus isolate the effect of entropic sources. It is stated that the segregation is dependent on the density, and for low density blends, the more flexible component segregates to the surface and at melt-like or liquid-like densities the stiffer component segregates to the surface. The flexible component used in the simulation does not have bond angle limitation in addition to excluded volume, however, that is not true for the stiff component. Excluded volume for a polymer chain means that a monomer along the polymer chain can not be in a position which is already filled by another monomer of the same polymer chain.

The bending potential of a stiff component could be derived as follows;

$$\beta U_B = \frac{\kappa}{2}(1 + \cos\theta)^2 \tag{4.7}$$

where β is equal to $\frac{1}{kT}$, k is the Boltzmann's constant, T is the temperature, κ is the bending constant, and θ is the bond angle.

Surface enrichment in polymer blends is studied as a function of packing and configurational effects. The competition between these two parameters affects the final result of the surface enrichment. It is stated that in low-density polymer blends, the loss of configurational entropy near the surface makes the polymer reluctant to stay at the surface.

However, in the liquid-like density polymer blends, the behavior would be totally different, since in this case the packing effect would be a dominant factor. At higher density, polymer molecules tend to pack against each other. When it comes to packing, the stiffer polymers find it easier to pack against each other. Hence, in this case, we would have surface enrichment in stiffer component [58].

In this work, density and packing effect was not considered as one of the parameters which play a role in segregation, thus, It would be nice to consider as many parameters to make the simulation closer to the real life.

4.2.4 Different parameters

In this work, as changing all the inputs makes the work daunting, we set some of them constant and focused on studying the effect of other inputs that we had. For example, in

this work, we study the binary polymer blends which are 50-50 in the bulk. However, a lot of blends that are applied in industry with different concentrations. Hence, we need to study the effect of changing concentration as well.

The other thing, which could be extended about our work, is the number of polymer components that we have in the blend. In this work, only a binary polymer blend is taken into account. However, In industry, we may deal with polymer blends with larger number of components. Changing other inputs can be the subject of new studies in this area.

4.2.5 Experiments

As was discussed in the introduction chapter, several experiments were designed to measure the surface segregation of polymer blends where one component is stiffer than the other. However, none of these experiments were free of problems. For example, some experimental methods rely on labeling one polymer component by deuterium. Although tracking the mentioned component becomes possible, there are some studies which show that in the isotopic binary polymer blend, the deuterated component always segregates to the surface [48, 55]. These findings reveal that labeling a polymer component will affect the segregation itself and it is not a reliable method for studying surface enrichment of polymer blend.

Although recently an experimental method [43], known as surface layer matrix-assisted laser desorption ionization time-of-flight (SL-MALDI-TOF-MS) [108, 109, 110], was applied to study the segregation of a polymer blend where polymer chains are different in length. The fact that makes this method unique is that there is no need for labeling one component. Besides, by the use of this experimental method, one could determine the molecular weight distribution. This experiment confirmed the simulation results qualitatively.

This method could be used to study the surface enrichment of polymer blends, where one polymer component is longer than the other, but there is no experiment to observe the surface segregation of polymer blends with different stiffness yet. Based on the results of this work, the shorter polymer component segregates to the surface, which is confirmed by experiments, but two other cases were studies in this work as well where one polymer component was flexible and the other was stiff. In the first case, the two components have the same contour length and in the second case, they have the same end-to-end distance, however, we are not able to confirm these results by the experiments.

There is a huge gap in this area which is lack of a viable experiment in this field. Experiments help us confirm the results predicted by theory or simulation qualitatively. Quantitative deviation could help us to enhance our assumptions to get them closer to

the real life. Hence, the other issue, which needs to be taken in this field, is designing a practical experiment.

References

[1] M. W. Matsen, "Self-consistent field theory and its applications," *Soft Matter*, vol. 1, 2006.

[2] J. P. Oliveira, A. R. Prado, W. J. Keijok, M. R. Ribeiro, M. J. Pontes, B. V. Nogueira, and M. C. Guimarães, "A helpful method for controlled synthesis of monodisperse gold nanoparticles through response surface modeling," *Arabian Journal of Chemistry*, vol. 13, no. 1, pp. 216–226, 2020.

[3] S. J. Park, D. Yong, Y. Kim, and J. U. Kim, "Numerical implementation of pseudo-spectral method in self-consistent mean field theory for discrete polymer chains," *The Journal of chemical physics*, vol. 150, no. 23, p. 234901, 2019.

[4] J. Colwill, "Introduction to polymers in sustainable engineering," *International Journal of Sustainable Engineering*, vol. 5, no. 1, pp. 2–2, 2012.

[5] J. R. Paddock, A. T. Maghasi, W. R. Heineman, and C. J. Seliskar, "Making and using a sensing polymeric material for cu2+: An introduction to polymers and chemical sensing," *Journal of chemical education*, vol. 82, no. 9, p. 1370, 2005.

[6] D. Knorr, "Use of chitinous polymers in food: a challenge for food research and development," *Food Technology (USA)*, 1984.

[7] G. A. Valencia, E. N. Zare, P. Makvandi, and T. J. Gutiérrez, "Self-assembled carbohydrate polymers for food applications: A review," *Comprehensive reviews in food science and food safety*, vol. 18, no. 6, pp. 2009–2024, 2019.

[8] J. Rydz, M. Musioł, B. Zawidlak-Wegrzyńska, and W. Sikorska, "Present and future of biodegradable polymers for food packaging applications," *Biopolymers for food design*, pp. 431–467, 2018.

[9] B. Tajeddin and M. Arabkhedri, "Polymers and food packaging," in *Polymer Science and Innovative Applications*, pp. 525–543, Elsevier, 2020.

[10] D. Hada, K. Rathore, T. Barupal, N. S. Chundawat, K. Sharma, and N. P. S. Chauhan, "Grafted biopolymers i: methodology and factors affecting grafting," in *Advanced Functional Polymers for Biomedical Applications*, pp. 21–42, Elsevier, 2019.

[11] R. Taherian and A. Kausar, *Electrical Conductivity in Polymer-Based Composites: Experiments, Modelling, and Applications*. William Andrew, 2018.

[12] M. Rayner, K. Östbring, and J. Purhagen, "Application of natural polymers in food," *Natural polymers*, pp. 115–161, 2016.

[13] D. R. Paul, *Polymer Blends Volume 1*, vol. 1. Elsevier, 2012.

[14] C. Koning, M. Van Duin, C. Pagnoulle, and R. Jerome, "Strategies for compatibilization of polymer blends," *Progress in polymer science*, vol. 23, no. 4, pp. 707–757, 1998.

[15] L. A. Utracki and C. A. Wilkie, *Polymer blends handbook*, vol. 1. Kluwer academic publishers Dordrecht, 2002.

[16] J. P. Donley, D. T. Wu, and G. H. Fredrickson, "On the control of surface enrichment in polymer blends and copolymers," *Macromolecules*, vol. 30, no. 7, pp. 2167–2174, 1997.

[17] D. T. Wu, G. H. Fredrickson, and J.-P. Carton, "Surface segregation in conformationally asymmetric polymer blends: Incompressibility and boundary conditions," *The Journal of chemical physics*, vol. 104, no. 16, pp. 6387–6397, 1996.

[18] T. R. Crompton, *Analysis of polymers: an introduction*. 1989.

[19] G. R. Strobl and G. R. Strobl, *The physics of polymers*, vol. 2. Springer, 1997.

[20] R. J. Young and P. A. Lovell, *Introduction to polymers*. CRC press, 2011.

[21] V. R. Gowariker, N. Viswanathan, and J. Sreedhar, *Polymer science*. New Age International, 1986.

[22] L. H. Sperling, *Introduction to physical polymer science*. John Wiley & Sons, 2005.

[23] M. Doi, *Introduction to polymer physics*. Oxford university press, 1996.

[24] A. Gurses, *Introduction to Polymer-Clay Nanocomposites*. CRC Press, 2015.

[25] L. A. Utracki, *Commercial polymer blends*. Springer Science & Business Media, 2013.

[26] L. Yu, K. Dean, and L. Li, "Polymer blends and composites from renewable resources," *Progress in polymer science*, vol. 31, no. 6, pp. 576–602, 2006.

[27] D. Paul and J. Barlow, "Polymer blends," *Journal of Macromolecular Science—Reviews in Macromolecular Chemistry*, vol. 18, no. 1, pp. 109–168, 1980.

[28] L. M. Robeson, "Polymer blends," *A Comprehensive Review*, 2007.

[29] M. Tambasco, J. Lipson, and J. S. Higgins, "Blend miscibility and the flory- huggins interaction parameter: a critical examination," *Macromolecules*, vol. 39, no. 14, pp. 4860–4868, 2006.

[30] F. S. Bates, "Polymer-polymer phase behavior," *Science*, vol. 251, no. 4996, pp. 898–905, 1991.

[31] M. Kinoshita, "Importance of translational, configurational entropy of water," in *Mechanism of Functional Expression of the Molecular Machines*, pp. 5–20, Springer, 2016.

[32] R. Gautam and W. D. Seider, "Computation of phase and chemical equilibrium: Part i. local and constrained minima in gibbs free energy," *AIChE Journal*, vol. 25, no. 6, pp. 991–999, 1979.

[33] M. Folkes and P. Hope, *Polymer blends and alloys*. Springer, 1993.

[34] K. Kehr and R. Kutner, "Random walk on a random walk," *Physica A: Statistical Mechanics and its Applications*, vol. 110, no. 3, pp. 535–549, 1982.

[35] R. J. Rubin, "Random-walk model of chain-polymer adsorption at a surface," *The Journal of Chemical Physics*, vol. 43, no. 7, pp. 2392–2407, 1965.

[36] M. Fixman, "Radius of gyration of polymer chains," *The Journal of Chemical Physics*, vol. 36, no. 2, pp. 306–310, 1962.

[37] A. Vega-Paz, F. d. J. Guevara-Rodríguez, J. Palomeque-Santiago, and N. V. Likhanova, "Polymer weight determination from numerical and experimental data of the reduced viscosity of polymer in brine," *Revista mexicana de física*, vol. 65, no. 4, pp. 321–327, 2019.

[38] A. Yethiraj, "Entropic and enthalpic surface segregation from blends of branched and linear polymers," *Physical review letters*, vol. 74, no. 11, p. 2018, 1995.

[39] A. Agrawal, "Surface tension of polymers," *Hatsopoulos Microfluids Laboratory, Department of Mechanical Engineering, Massachusetts Institute of Technology*, 2005.

[40] P. Mahmoudi, "Entropic segregation at surfaces of polymer melts," 2018.

[41] I. Szleifer, "Statistical thermodynamics of polymers near surfaces," *Current Opinion in Colloid & Interface Science*, vol. 1, no. 3, pp. 416–423, 1996.

[42] I. C. Henderson and N. Clarke, "On modelling surface directed spinodal decomposition," *Macromolecular theory and simulations*, vol. 14, no. 7, pp. 435–443, 2005.

[43] J. A. Hill, K. J. Endres, P. Mahmoudi, M. W. Matsen, C. Wesdemiotis, and M. D. Foster, "Detection of surface enrichment driven by molecular weight disparity in virtually monodisperse polymers," *ACS Macro Letters*, vol. 7, no. 4, pp. 487–492, 2018.

[44] A. Hariharan, S. K. Kumar, and T. P. Russell, "Surface segregation in binary polymer mixtures: a lattice model," *Macromolecules*, vol. 24, no. 17, pp. 4909–4917, 1991.

[45] S. K. Kumar and I. Szleifer, "The role of intefacial diffuseness on surface segregation from polymer blends," *Soft Materials*, vol. 5, no. 2-3, pp. 75–85, 2007.

[46] M. Stamm and J.-U. Sommer, "Entropy and enthalpy at play," *Nature materials*, vol. 6, no. 4, pp. 260–261, 2007.

[47] S. K. Kumar, A. Yethiraj, K. S. Schweizer, and F. A. Leermakers, "The effects of local stiffness disparity on the surface segregation from binary polymer blends," *The Journal of chemical physics*, vol. 103, no. 23, pp. 10332–10346, 1995.

[48] R. A. Jones, E. J. Kramer, M. H. Rafailovich, J. Sokolov, and S. A. Schwarz, "Surface enrichment in an isotopic polymer blend," *Physical review letters*, vol. 62, no. 3, p. 280, 1989.

[49] V. S. Minnikanti, Z. Qian, and L. A. Archer, "Surface segregation and surface tension of polydisperse polymer melts," *The Journal of chemical physics*, vol. 126, no. 14, p. 144905, 2007.

[50] J. Van der Gucht, N. Besseling, and G. Fleer, "Surface segregation in polydisperse polymer melts," *Macromolecules*, vol. 35, no. 17, pp. 6732–6738, 2002.

[51] M. Sikka, N. Singh, A. Karim, F. S. Bates, S. K. Satija, and C. F. Majkrzak, "Entropy-driven surface segregation in block copolymer melts," *Physical review letters*, vol. 70, no. 3, p. 307, 1993.

[52] W. Zhao, X. Zhao, M. Rafailovich, J. Sokolov, R. Composto, S. Smith, T. Russell, W. Dozier, T. Mansfield, and M. Satkowski, "Segregation of chain ends to polymer melt surfaces and interfaces," *Macromolecules*, vol. 26, no. 3, pp. 561–562, 1993.

[53] L. Norton, E. Kramer, F. S. Bates, M. Gehlsen, R. Jones, A. Karim, G. Felcher, and R. Kleb, "Neutron reflectometry study of surface segregation in an isotopic poly (ethylenepropylene) blend: deviation from mean-field theory," *Macromolecules*, vol. 28, no. 25, pp. 8621–8628, 1995.

[54] S. Schwarz, B. Wilkens, M. Pudensi, M. Rafailovich, J. Sokolov, X. Zhao, W. Zhao, X. Zheng, T. Russell, and R. Jones, "Studies of surface and interface segregation in polymer blends by secondary ion mass spectrometry," *Molecular Physics*, vol. 76, no. 4, pp. 937–950, 1992.

[55] A. Hariharan, S. K. Kumar, and T. P. Russell, "Reversal of the isotopic effect in the surface behavior of binary polymer blends," *The Journal of chemical physics*, vol. 98, no. 5, pp. 4163–4173, 1993.

[56] G. H. Fredrickson and J. P. Donley, "Influence of broken conformational symmetry on the surface enrichment of polymer blends," *The Journal of chemical physics*, vol. 97, no. 12, pp. 8941–8946, 1992.

[57] S. Stepanow and A. A. Fedorenko, "Surface segregation of conformationally asymmetric polymer blends," *Physical Review E*, vol. 73, no. 3, p. 031801, 2006.

[58] A. Yethiraj, S. Kumar, A. Hariharan, and K. S. Schweizer, "Surface segregation in polymer blends due to stiffness disparity," *The Journal of chemical physics*, vol. 100, no. 6, pp. 4691–4694, 1994.

[59] P. Mahmoudi and M. Matsen, "Entropic segregation of short polymers to the surface of a polydisperse melt," *The European Physical Journal E*, vol. 40, no. 10, p. 85, 2017.

[60] F. Schmid, "Self-consistent-field theories for complex fluids," *Journal of Physics: Condensed Matter*, vol. 10, no. 37, p. 8105, 1998.

[61] M. Whitmore and J. Vavasour, "Self-consistent field theory of block copolymers and block copolymer blends," *Acta polymerica*, vol. 46, no. 5, pp. 341–360, 1995.

[62] V. Faraoni, M. Grosso, S. Crescitelli, and P. Maffettone, "The rigid-rod model for nematic polymers: an analysis of the shear flow problem," *Journal of Rheology*, vol. 43, no. 3, pp. 829–843, 1999.

[63] H. G. Chae and S. Kumar, "Rigid-rod polymeric fibers," *Journal of Applied Polymer Science*, vol. 100, no. 1, pp. 791–802, 2006.

[64] D. J. Sikkema and V. L. Lishinsky, "Rigid rod polymer based on pyridobisimidazole," Oct. 1997. US Patent 5,674,969.

[65] A. Baumgärtner and K. Binder, "Monte carlo studies on the freely jointed polymer chain with excluded volume interaction," *The Journal of Chemical Physics*, vol. 71, no. 6, pp. 2541–2545, 1979.

[66] A. Baumgärtner, "Statics and dynamics of the freely jointed polymer chain with lennard-jones interaction," *The Journal of Chemical Physics*, vol. 72, no. 2, pp. 871–879, 1980.

[67] A. McMullen, M. Holmes-Cerfon, F. Sciortino, A. Y. Grosberg, and J. Brujic, "Freely jointed polymers made of droplets," *Physical review letters*, vol. 121, no. 13, p. 138002, 2018.

[68] Y. J. Sheng, A. Z. Panagiotopoulos, S. K. Kumar, and I. Szleifer, "Monte carlo calculation of phase equilibria for a bead-spring polymeric model," *Macromolecules*, vol. 27, no. 2, pp. 400–406, 1994.

[69] R. Bird, P. Dotson, and N. Johnson, "Polymer solution rheology based on a finitely extensible bead—spring chain model," *Journal of Non-Newtonian Fluid Mechanics*, vol. 7, no. 2-3, pp. 213–235, 1980.

[70] A. S. Lodge and Y.-J. Wu, "Constitutive equations for polymer solutions derived from the bead/spring model of rouse and zimm," *Rheologica Acta*, vol. 10, no. 4, pp. 539–553, 1971.

[71] H.-X. Zhou, "A gaussian-chain model for treating residual charge–charge interactions in the unfolded state of proteins," *Proceedings of the National Academy of Sciences*, vol. 99, no. 6, pp. 3569–3574, 2002.

[72] H.-X. Zhou, "Direct test of the gaussian-chain model for treating residual charge-charge interactions in the unfolded state of proteins," *Journal of the American Chemical Society*, vol. 125, no. 8, pp. 2060–2061, 2003.

[73] A. Skvortsov, B. Belen'kii, E. Gankina, and M. Tennikov, "Agreement between the behaviour of a real macromolecule and a gaussian chain during adsorption in pores," *Polymer Science USSR*, vol. 20, no. 3, pp. 768–778, 1978.

[74] C. Bouchiat, M. D. Wang, J.-F. Allemand, T. Strick, S. Block, and V. Croquette, "Estimating the persistence length of a worm-like chain molecule from force-extension measurements," *Biophysical journal*, vol. 76, no. 1, pp. 409–413, 1999.

[75] H.-P. Hsu, W. Paul, and K. Binder, "Polymer chain stiffness vs. excluded volume: A monte carlo study of the crossover towards the worm-like chain model," *EPL (Europhysics Letters)*, vol. 92, no. 2, p. 28003, 2010.

[76] M. Bohdanecky, "New method for estimating the parameters of the wormlike chain model from the intrinsic viscosity of stiff-chain polymers," *Macromolecules*, vol. 16, no. 9, pp. 1483–1492, 1983.

[77] A. E. Hoyt and B. C. Benicewicz, "Rigid rod molecules as liquid crystal thermosets. i. rigid rod amides," *Journal of Polymer Science Part A: Polymer Chemistry*, vol. 28, no. 12, pp. 3403–3415, 1990.

[78] G. Fredrickson *et al.*, *The equilibrium theory of inhomogeneous polymers*, vol. 134. Oxford University Press on Demand, 2006.

[79] R. L. Burden and J. D. Faires, "Numerical analysis (nineth edition)," 2010.

[80] S. Blaber, P. Mahmoudi, R. Spencer, and M. Matsen, "Effect of chain stiffness on the entropic segregation of chain ends to the surface of a polymer melt," *The Journal of chemical physics*, vol. 150, no. 1, p. 014904, 2019.

[81] S. Blaber, "Equilibrium phase behaviour of liquid crystalline polymer brushes," Master's thesis, University of Waterloo, 2019.

[82] Q. Liang, J. Li, P. Zhang, and J. Z. Chen, "Modified diffusion equation for the wormlike-chain statistics in curvilinear coordinates," *The Journal of chemical physics*, vol. 138, no. 24, p. 244910, 2013.

[83] D. Zill, W. S. Wright, and M. R. Cullen, *Advanced engineering mathematics*. Jones & Bartlett Learning, 2016.

[84] P. McCarthy, J. Sayre, and B. Shawyer, "Generalized legendre polynomials," *Journal of Mathematical Analysis and Applications*, vol. 177, no. 2, pp. 530–537, 1993.

[85] G. Dattoli, P. E. Ricci, and C. Cesarano, "A note on legendre polynomials," *International Journal of Nonlinear Sciences and Numerical Simulation*, vol. 2, no. 4, pp. 365–370, 2001.

[86] G. Sansone, "Orthogonal functions," 1959.

[87] L. C. Andrews, *Special functions of mathematics for engineers*, vol. 49. Spie Press, 1998.

[88] E. W. Weisstein, "Legendre polynomial," 2002.

[89] Y. Chang and G. Corliss, "Atomft: solving odes and daes using taylor series," *Computers & Mathematics with Applications*, vol. 28, no. 10-12, pp. 209–233, 1994.

[90] J. R. Scott, "Solving ode initial value problems with implicit taylor series methods," 2000.

[91] B. Vorselaars, J. U. Kim, T. L. Chantawansri, G. H. Fredrickson, and M. W. Matsen, "Self-consistent field theory for diblock copolymers grafted to a sphere," *Soft Matter*, vol. 7, no. 11, pp. 5128–5137, 2011.

[92] M. W. Matsen, "Fast and accurate scft calculations for periodic block-copolymer morphologies using the spectral method with anderson mixing," *The European Physical Journal E*, vol. 30, no. 4, pp. 361–369, 2009.

[93] R. B. Thompson, K. O. Rasmussen, and T. Lookman, "Improved convergence in block copolymer self-consistent field theory by anderson mixing," *The Journal of chemical physics*, vol. 120, no. 1, pp. 31–34, 2004.

[94] P. Stasiak and M. Matsen, "Efficiency of pseudo-spectral algorithms with anderson mixing for the scft of periodic block-copolymer phases," *The European Physical Journal E*, vol. 34, no. 10, pp. 1–9, 2011.

[95] N. Maurits, J. Fraaije, P. Altevogt, and O. Evers, "Simple numerical quadrature rules for gaussian chain polymer density functional calculations in 3d and implementation on parallel platforms," *Computational and Theoretical Polymer Science*, vol. 6, pp. 1–8, 1996.

[96] R. W. Ogden, G. Saccomandi, and I. Sgura, "On worm-like chain models within the three-dimensional continuum mechanics framework," *Proceedings of the Royal Society A: Mathematical, Physical and Engineering Sciences*, vol. 462, no. 2067, pp. 749–768, 2006.

[97] H. Yamakawa and J. Shimada, "Stiffness and excluded-volume effects in polymer chains," *The Journal of chemical physics*, vol. 83, no. 5, pp. 2607–2611, 1985.

[98] A. Milchev and K. Binder, "How does stiffness of polymer chains affect their adsorption transition?," *The Journal of chemical physics*, vol. 152, no. 6, p. 064901, 2020.

[99] R. F. Boyer and R. L. Miller, "Polymer chain stiffness parameter, σ, and cross-sectional area per chain," *Macromolecules*, vol. 10, no. 5, pp. 1167–1169, 1977.

[100] C. A. Joziasse, H. Veenstra, D. W. Grijpma, and A. J. Pennings, "On the chain stiffness of poly (lactide) s," *Macromolecular Chemistry and Physics*, vol. 197, no. 7, pp. 2219–2229, 1996.

[101] J. J. Burgos-Marmol, O. Alvarez-Machancoses, and A. Patti, "Modeling the effect of polymer chain stiffness on the behavior of polymer nanocomposites," *The Journal of Physical Chemistry B*, vol. 121, no. 25, pp. 6245–6256, 2017.

[102] C. A. GLOVER, "Determination of number-average molecular weights by ebulliometry," ACS Publications, 1973.

[103] H. G. Barth and J. W. Mays, *Modern methods of polymer characterization*, vol. 115. John Wiley & Sons, 1991.

[104] P. E. Slade, *Polymer Molecular Weights,(2 Part)*, vol. 4. CRC Press, 1975.

[105] J. U. Izunobi and C. L. Higginbotham, "Polymer molecular weight analysis by 1h nmr spectroscopy," *Journal of Chemical Education*, vol. 88, no. 8, pp. 1098–1104, 2011.

[106] J. A. Manson, *Polymer blends and composites*. Springer Science & Business Media, 2012.

[107] H. Ng, A. Allegrezza, R. Seymour, and S. L. Cooper, "Effect of segment size and polydispersity on the properties of polyurethane block polymers," *Polymer*, vol. 14, no. 6, pp. 255–261, 1973.

[108] S.-F. Wang, X. Li, R. L. Agapov, C. Wesdemiotis, and M. D. Foster, "Probing surface concentration of cyclic/linear blend films using surface layer maldi-tof mass spectrometry," *ACS Macro Letters*, vol. 1, no. 8, pp. 1024–1027, 2012.

[109] I. Smirnov, X. Zhu, T. Taylor, Y. Huang, P. Ross, I. Papayanopoulos, S. Martin, and D. Pappin, "Suppression of α-cyano-4-hydroxycinnamic acid matrix clusters and reduction of chemical noise in maldi-tof mass spectrometry," *Analytical chemistry*, vol. 76, no. 10, pp. 2958–2965, 2004.

[110] Z. Liu and K. L. Schey, "Fragmentation of multiply-charged intact protein ions using maldi tof-tof mass spectrometry," *Journal of the American Society for Mass Spectrometry*, vol. 19, no. 2, pp. 231–238, 2008.

[111] G. H. Fredrickson, *The equilibrium theory of inhomogeneous polymers*. Oxford : Clarendon, 2006.

[112] M. Sikka, N. Singh, A. Karim, F. S. Bates, S. K. Satija, and C. F. Majkrzak, "Entropy-driven surface segregation in block copolymer melts," *Phys. Rev. Lett.*, vol. 70, pp. 307–310, Jan 1993.

[113] M. Matsen, *Self-Consistent Field Theory and Its Applications*. 2017.

[114] I. Teraoka and P. Solutions, "An introduction to physical properties," 2002.

[115] R. K. Tyson and B. W. Frazier, *Field guide to adaptive optics*. SPIE Press,, 2012.

[116] T. Kawakatsu, *Statistical physics of polymers: an introduction*. Springer Science & Business Media, 2013.

[117] D. C. Morse and G. H. Fredrickson, "Semiflexible polymers near interfaces," *Physical review letters*, vol. 73, no. 24, p. 3235, 1994.

[118] U. Steiner, J. Klein, E. Eiser, A. Budkowski, and L. J. Fetters, "Complete wetting from polymer mixtures," *Science*, vol. 258, no. 5085, pp. 1126–1129, 1992.

[119] J. Baschnagel, H. Meyer, J. Wittmer, I. Kulić, H. Mohrbach, F. Ziebert, G.-M. Nam, N.-K. Lee, and A. Johner, "Semiflexible chains at surfaces: Worm-like chains and beyond," *polymers*, vol. 8, no. 8, p. 286, 2016.

[120] N. P. Adhikari, R. Auhl, and E. Straube, "Interfacial properties of flexible and semi-flexible polymers," *Macromolecular theory and simulations*, vol. 11, no. 3, pp. 315–325, 2002.

[121] T. Kajiyama, K. Tanaka, and A. Takahara, "Surface segregation of the higher surface free energy component in symmetric polymer blend films," *Macromolecules*, vol. 31, no. 11, pp. 3746–3749, 1998.

[122] V. Ivanov, J. Martemyanova, A. Rodionova, and M. Stukan, "Computer simulation of stiff-chain polymers," *Polymer Science Series C*, vol. 55, no. 1, pp. 4–22, 2013.

[123] E. Chiellini and R. Solaro, *Biodegradable polymers and plastics*. Springer Science & Business Media, 2012.

[124] L. Rupprecht, *Conductive polymers and plastics: in industrial applications*. William Andrew, 1999.

[125] D. Walton and A. Mayes, "Entropically driven segregation in blends of branched and linear polymers," *Physical Review E*, vol. 54, no. 3, p. 2811, 1996.

[126] M. Haraguchi, T. Hirai, M. Ozawa, K. Miyaji, and K. Tanaka, "Hydrophobic acrylic hard coating by surface segregation of hyper-branched polymers," *Applied surface science*, vol. 266, pp. 235–238, 2013.

[127] R. Alamo, W. Graessley, R. Krishnamoorti, D. Lohse, J. Londono, L. Mandelkern, F. Stehling, and G. Wignall, "Small angle neutron scattering investigations of melt miscibility and phase segregation in blends of linear and branched polyethylenes as a function of the branch content," *Macromolecules*, vol. 30, no. 3, pp. 561–566, 1997.

[128] D. T. Wu and G. H. Fredrickson, "Effect of architecture in the surface segregation of polymer blends," *Macromolecules*, vol. 29, no. 24, pp. 7919–7930, 1996.

[129] M. Diez-Minguito, J. Marro, and P. L. Garrido, "On the similarities and differences between lattice and off–lattice models of driven fluids," *The European Physical Journal Special Topics*, vol. 143, no. 1, pp. 269–272, 2007.

[130] W. E. Hart and S. Istrail, "Lattice and off-lattice side chain models of protein folding (extended abstract) linear time structure prediction better than 86% of optimal," in *Proceedings of the first annual international conference on Computational molecular biology*, pp. 137–146, 1997.

[131] R. S. Porter and J. F. Johnson, "The entanglement concept in polymer systems," *Chemical Reviews*, vol. 66, no. 1, pp. 1–27, 1966.

[132] H. Tsukeshiba, M. Huang, Y.-H. Na, T. Kurokawa, R. Kuwabara, Y. Tanaka, H. Furukawa, Y. Osada, and J. P. Gong, "Effect of polymer entanglement on the toughening of double network hydrogels," *The Journal of Physical Chemistry B*, vol. 109, no. 34, pp. 16304–16309, 2005.

[133] N. Heymans, "A novel look at models for polymer entanglement," *Macromolecules*, vol. 33, no. 11, pp. 4226–4234, 2000.

[134] D. Zill, W. S. Wright, and M. R. Cullen, *Advanced engineering mathematics*. Jones & Bartlett Learning, 2011.

[135] H.-X. Zhou, "Residual charge interactions in unfolded staphylococcal nuclease can be explained by the gaussian-chain model," *Biophysical journal*, vol. 83, no. 6, pp. 2981–2986, 2002.

[136] J. Elman, B. Johs, T. Long, and J. Koberstein, "A neutron reflectivity investigation of surface and interface segregation of polymer functional end groups," *Macromolecules*, vol. 27, no. 19, pp. 5341–5349, 1994.

[137] P. Cifra, F. Karasz, and W. MacKnight, "Surface segregation in polymer blends: a monte carlo simulation," *Macromolecules*, vol. 25, no. 19, pp. 4895–4901, 1992.

[138] H. Alam, C. B. Park, and R. B. Thompson, "An off-lattice model of the sanchez-lacombe equation of state for polymers with finite flexibility," *Polymer*, p. 123334, 2020.

[139] H. Alam, "An o-lattice model of the sanchez-lacombe equation of state for polymers with finite flexibility," pp. 31–39, 2020.

[140] E. Neau, "A consistent method for phase equilibrium calculation using the sanchez–lacombe lattice–fluid equation-of-state," *Fluid Phase Equilibria*, vol. 203, no. 1-2, pp. 133–140, 2002.

[141] E. Kiran, Y. Xiong, and W. Zhuang, "Modeling polyethylene solutions in near and supercritical fluids using the sanchez-lacombe model," *The Journal of Supercritical Fluids*, vol. 6, no. 4, pp. 193–203, 1993.

[142] K. Gauter and R. A. Heidemann, "Modeling polyethylene-solvent mixtures with the sanchez–lacombe equation," *Fluid phase equilibria*, vol. 183, pp. 87–97, 2001.

[143] C. Panayiotou and J. Vera, "The quasi-chemical approach for non-randomness in liquid mixtures. expressions for local surfaces and local compositions with an application to polymer solutions," *Fluid Phase Equilibria*, vol. 5, no. 1-2, pp. 55–80, 1980.

[144] B. H. Chang, Y. C. Bae, A. R. Imre, and Y. K. Sun, "Polymer–polymer miscibility: generalized double lattice model," *Polymer*, vol. 45, no. 23, pp. 8067–8074, 2004.

[145] R. Brak, A. Owczarek, and A. Rechnitzer, "Exact solutions of lattice polymer models," *Journal of mathematical chemistry*, vol. 45, no. 1, pp. 39–57, 2009.

[146] D. Bedrov, G. D. Smith, K. F. Freed, and J. Dudowicz, "A comparison of self-assembly in lattice and off-lattice model amphiphile solutions," *The Journal of chemical physics*, vol. 116, no. 12, pp. 4765–4768, 2002.

[147] J. Dautenhahn and C. K. Hall, "Monte carlo simulation of off-lattice polymer chains: effective pair potentials in dilute solution," *Macromolecules*, vol. 27, no. 19, pp. 5399–5412, 1994.

[148] S. Metzger, M. Müller, K. Binder, and J. Baschnagel, "Adsorption transition of a polymer chain at a weakly attractive surface: Monte carlo simulation of off-lattice models," *Macromolecular theory and simulations*, vol. 11, no. 9, pp. 985–995, 2002.

[149] L.-Y. Shy, Y. Leung, and B. Eichinger, "Critical exponents for off-lattice gelation of polymer chains," *Macromolecules*, vol. 18, no. 5, pp. 983–986, 1985.

[150] V. Siracusa, P. Rocculi, S. Romani, and M. Dalla Rosa, "Biodegradable polymers for food packaging: a review," *Trends in Food Science & Technology*, vol. 19, no. 12, pp. 634–643, 2008.

[151] S. Mangaraj, A. Yadav, L. M. Bal, S. Dash, and N. K. Mahanti, "Application of biodegradable polymers in food packaging industry: a comprehensive review," *Journal of Packaging Technology and Research*, vol. 3, no. 1, pp. 77–96, 2019.

[152] J. Bisquert, G. G. Belmonte, F. F. Santiago, N. S. Ferriols, M. Yamashita, and E. C. Pereira, "Application of a distributed impedance model in the analysis of conducting polymer films," *Electrochemistry Communications*, vol. 2, no. 8, pp. 601–605, 2000.

[153] E. Raphael, C. O. Avellaneda, B. Manzolli, and A. Pawlicka, "Agar-based films for application as polymer electrolytes," *Electrochimica Acta*, vol. 55, no. 4, pp. 1455–1459, 2010.

[154] S. K. Park, J. I. Han, W. K. Kim, and M. G. Kwak, "Deposition of indium–tin-oxide films on polymer substrates for application in plastic-based flat panel displays," *Thin Solid Films*, vol. 397, no. 1-2, pp. 49–55, 2001.

[155] M. Matsen and P. Mahmoudi, "Segregation of chain ends to the surface of a polymer melt," *The European Physical Journal E*, vol. 37, no. 8, pp. 1–8, 2014.

[156] V. Padmanabhan, A. L. Frischknecht, and M. E. Mackay, "Effect of chain stiffness on nanoparticle segregation in polymer/nanoparticle blends near a substrate," *Macromolecular Theory and Simulations*, vol. 21, no. 2, pp. 98–105, 2012.

[157] A. Budkowski, "Interfacial phenomena in thin polymer films: phase coexistence and segregation," *Interfaces Crystallization Viscoelasticity*, pp. 1–111, 1999.

[158] J. M. Polson and L. G. Montgomery, "Polymer segregation under confinement: Free energy calculations and segregation dynamics simulations," *The Journal of chemical physics*, vol. 141, no. 16, p. 164902, 2014.

[159] P. Teyssie, "Polymer blends: from molecular structure through morphology to controlled bulk properties," in *Makromolekulare Chemie. Macromolecular Symposia*, vol. 22, pp. 83–94, Wiley Online Library, 1988.

[160] Y. Ding and A. Sokolov, "Comment on the dynamic bead size and kuhn segment length in polymers: Example of polystyrene," *Journal of Polymer Science Part B: Polymer Physics*, vol. 42, no. 18, pp. 3505–3511, 2004.

[161] N. Saitô, K. Takahashi, and Y. Yunoki, "The statistical mechanical theory of stiff chains," *Journal of the Physical Society of Japan*, vol. 22, no. 1, pp. 219–226, 1967.

[162] K. Sugeno, S. Kokubun, and H. Saito, "Ucst type phase boundary and accelerated crystallization in ptt/pet blends," *Polymers*, vol. 12, no. 11, p. 2730, 2020.

[163] Y. S. N. Lipatov and A. E. A. Evtikhievich, "Thermodynamics of polymer blends/yuri s. lipatov, anatoly e. nesterov.," *Polymer thermodynamics library; 1.*

APPENDICES

Appendix A

Tridiagonal matrix

In a tridiagonal matrix, all the elements are zero except for diagonal elements and the first diagonal below and above the main diagonal.

$$A = \begin{pmatrix} a_{11} & a_{12} & 0 & \cdots\cdots & 0 \\ a_{21} & a_{22} & a_{23} & \ddots & \vdots \\ 0 & \ddots & \ddots & \ddots & 0 \\ \vdots & \ddots & \ddots & \ddots & a_{n-1,n} \\ 0 & \cdots\cdots & 0 & a_{n,n-1} & a_{nn} \end{pmatrix}$$

One can write a three diagonal matrix in the form of product of two other tridiagonal matrices as follows;

$$A = LU \tag{A.1}$$

$$L = \begin{pmatrix} l_{11} & 0 & \cdots & \cdots & 0 \\ l_{21} & l_{22} & \ddots & & \vdots \\ 0 & \ddots & \ddots & \ddots & \vdots \\ \vdots & \ddots & \ddots & \ddots & 0 \\ 0 & \cdots\cdots & 0 & l_{n,n-1} & l_{n,n} \end{pmatrix}$$

$$U = \begin{pmatrix} 1 & u_{12} & 0 & \cdots\cdots & 0 \\ 0 & 1 & u_{23} & \ddots & \vdots \\ \vdots & \ddots & \ddots & \ddots & 0 \\ \vdots & & \ddots & \ddots & u_{n-1,n} \\ 0 & \cdots & \cdots & 0 & 1 \end{pmatrix}$$

Our first step is how to calculate L and U elements based on A elements. By multiplying L and U, we have;

$$a_{11} = l_{11} \tag{A.2}$$

$$a_{i,i-1} = l_{i,i-1} \tag{A.3}$$

$$a_{i,i} = l_{i,i-1}u_{i-1,i} + l_{ii} \tag{A.4}$$

$$a_{i,i+1} = l_{i,i}u_{i,i+1} \tag{A.5}$$

The above formulas could be rearranged to calculate L and U elements. Initially, we set $l_{11} = a_{11}$ and $u_{12} = \frac{a_{12}}{l_{11}}$ also we know that $l_{i,i-1} = a_{i,i-1}$ and after that other elements should be derived in this way;

$$l_{i,i} = a_{i,i} - l_{i,i-1}u_{i-1,i} \tag{A.6}$$

Now that $l_{i,i}$ is known, we can calculate $u_{i,i+1}$;

$$u_{i,i+1} = \frac{a_{i,i+1}}{l_{i,i}} \tag{A.7}$$

Until here L and U are defined and we can write matrix A in the form of the product of L and U. Now let's assume that $Ax = r$ is the equation that we tend to solve. This equation can be written in this way;

$$LUx = r \tag{A.8}$$

If we assume that $Ux = \rho$ then we could write equation [A.8] in this way, $L\rho = r$, hence we could solve for ρ first and after calculating that solve for x in equation, $Ux = \rho$.
With this in mind, we can illustrate the procedure for solving this equation, which is the

final objective of this appendix;

$$Aq^{i+1} = Bq^{i} \tag{A.9}$$